pH Sensitive Polymers for Improving Reservoir Sweep and Conformance

Semiannual Progress Report

May 1, 2006 to September 30, 2006

By
Mukul Sharma
Steve Bryant
Chun Huh

Work performed under Contract DE-FC26-04NT15520
Prepared for the U.S. Department of Energy

Betty Felber, Project Manager
U.S. Department of Energy
National Energy Technology Laboratory
One West 3rd Street, Suite 1400
Tulsa, OK 74103
918 699 2063

Prepared by

The University of Texas
Center for Petroleum and Geosystems Engineering
Austin, Texas 78712

Objectives

The overall research objective is to develop a low-cost, pH triggered polymer for use in polymer flooding to improve reservoir sweep efficiency and reservoir conformance in chemical flooding. The use of this polymer in conjunction with CO_2 flooding will be investigated in detail since a combination of the two offers some unique synergistic benefits. The specific objectives of the proposed work are:

1. To investigate changes in rheological properties of the solution as a function of polymer properties, pH, salt/brine composition, polymer concentration, temperature and lithology of the reservoir.
2. To assess the effectiveness as a mobility control agent for conformance control through core-flow tests, and long-sand-pack tests.
3. To evaluate polymer performance as a mobility and conformance control agent for CO_2 flooding applications.
4. Modify existing chemical flooding simulators to incorporate the specific pH dependent properties of the polymer so that effective polymer / CO_2 floods can be designed for different lithologies and reservoir conditions.

The tasks proposed above will allow the novel application of pH-sensitive polymers as effective mobility and conformance control agents for increasing the volumetric sweep efficiency of chemical floods.

RESULTS OF WORK DURING REPORTING PERIOD

Task 1. Polymer Characterization for Subsurface Application:

A laboratory rheological characterization was completed on a wide variety of aqueous polymers in terms of their salt compatibility and pH sensitivity (see Appendix I). The objective of this investigation was to find polymers that can be transported more effectively than the Carbopol polymers now being used.

Task 2. Core-Flow Tests for Polymer Propagation:

During this period, we have focused on polymer injection into fractured formations (Task 3). In view of the fact that a large polymer retention has been observed in low-permeability rocks (**SPE 99656**, "Transport of a pH-Sensitive Polymer in Porous Media for Novel Mobility Control Applications"), we decided to put Task 2 on hold, and re-visit Task 1 to find a polymer that can be transported in tight rocks with less retention.

Task 3. Conformance Control and Sweep in Heterogeneous Formations

Sandstone and carbonate cores were prepared with an embedded artificial fracture, and core flow experiments were carried out to investigate the possibility of profile control in heterogeneous formations (fractures being an extreme example of heterogeneity).

Our preliminary progress is described in detail in Appendix II.

Task 4. Long Sand Pack Tests for Polymer and pH Propagation

During this period, our focus was on the injection of polymer into the fractured formations (Task 3). In view of the fact that a large polymer retention has been observed in low-permeability rocks (SPE 99656, "Transport of a pH-Sensitive Polymer in Porous Media for Novel Mobility Control Applications"), we decided to put Task 4 on hold and re-visit Task 1 to find a polymer that can be transported with less retention in tight rocks.

Task 5. Polymer Assisted CO_2 WAG Process:

No work was done on this task during this time period.

Task 6. Simulation of Potential Sweep Improvement with pH-triggered Polymer

The viscosity model developed for the pH sensitive polymer (**SPE 96914**, "A Rheological Model for pH Sensitive Ionic Polymer Solutions for Optimal Mobility Control Applications") has been implemented into CMG's compositional simulator GEM. The validation testing of the viscosity model in GEM has been conducted as described in detail in **Appendix III**.

Employing the newly developed polymer option of GEM, and in order to obtain the geochemical parameters that are needed for field-scale screening simulations, we carried out a series of history-matching simulations for the acid-injection corefloods that we performed earlier. Details of this history-matching effort are described in **Appendix IV**.

Also employing the newly developed polymer option of GEM, some preliminary field-scale simulations were conducted to examine the benefit of using the pH-sensitive polymer. Details of the field-scale simulations are described in **Appendix V**.

In view of the complexity of the GEM simulations with complicated geochemical features, and the polymer option, we deemed it worthwhile to investigate simple analytical solutions for the idealized reservoirs, which consist of multiple parallel layers with no crossflow between them. The study provided valuable insight in preparing appropriate GEM simulation cases for the process screening studies. Details of this analytical approach are described in **Appendix VI**.

Another modeling effort we are pursuing is the development of a simplified software program that can be used for a preliminary design of pH-sensitive polymer bank size and concentration. The program could be employed for efficient computation of polymer propagation and its gelation in the reservoir. Again, the reservoir is assumed to consist of multiple parallel layers with no crossflow between them. Details of this simplified computational approach are described in **Appendix VII**.

Appendix I

Laboratory Characterization of Various Polymers

As shown in the previous report, cross-linked polyacrylic acid polymer has very good pH-sensitivity. However, it also shows relatively high adsorption and mechanical filtration during propagation. Another concern is that cross-linked polyacrylic acid can block the entrance of low permeability zone which is expected to be swept by subsequent-injected water.

The best polymer candidate for this application would fulfill the following three conditions.

- Salt compatibility in solution preparation
- pH-sensitivity
- Transport capability

Therefore, we have tried to find other polymers which can satisfy the above conditions. In this research, we want to find polymers which show an increase in viscosity of 20 to 30 times as pH is increased with only a small reduction in permeability when flowed through a core.

I.1. Polymer Screening Step

As a first step, various types of polymers were screened. Table 1 summarizes the polymers which have been evaluated and the test results. The results demonstrate that cross-linked polyacrylic acid and non-cross-linked polyacrylic acid polymers have relatively poor transport capability (much adsorption and mechanical filtration). On the other hand, emulsion cross-linked polyacrylic acid is incompatible with salt, which means that it precipitates with salt during solution preparation.

Table I.1. Polymer Screening Results

	Dispersibility	Salt Compatibility	pH sensitivity	Transportability
Cross-linked polyacrylic acid	Δ	Δ	O	Δ
Uncross-linked polyacrylic acid	O	O	Δ	Δ
Emulsion polymer		X		
HPAM	O	O	Δ	Future

Note: O: good, Δ: Intermediate, X: Bad

The results show that partially hydrolyzed polyacrylamide (HPAM), which is widely used in oilfield application, shows satisfactory pH sensitivity. Please note that this is not a cross-linked polymer. HPAM has two different functional groups around its back bone – carboxyl groups and amino groups. Carboxyl groups can be negatively charged or neutral depending on the hydrogen ion concentration (pH) in the solution. On the other hand, amino groups are less sensitive to pH.

I.2. pH sensitivity of HPAM

Laboratory experiments on the viscosity of HPAM polymers with different degrees of commercially-available hydrolysis have been performed. Figure 1 shows the viscosity dependence of four HPAM polymers which have different degrees of hydrolysis as a function of pH at a specific shear rate (3 rpm). It is clear that pure polyacrylic acid (100% degree of hydrolysis) has a relatively large viscosity change. On the other hand, pure polyacrylamide (zero degree of hydrolysis) has no viscosity sensitivity as a function of pH. Another interesting point is that polymer with a high degree of hydrolysis shows lower viscosity at low pH than polymers with a low degree of hydrolysis. According to the literature, polyacrylamide shows good transport with only a small permeability reduction. Therefore, we tentatively decided to find a polymer with an intermediate degree of hydrolysis for this application.

Figure 1. SUPERPOSED VISCOSITY VS PH AT 3 RPM
(0.5% Polymer Prepared in 0.5% NaCl Brine)

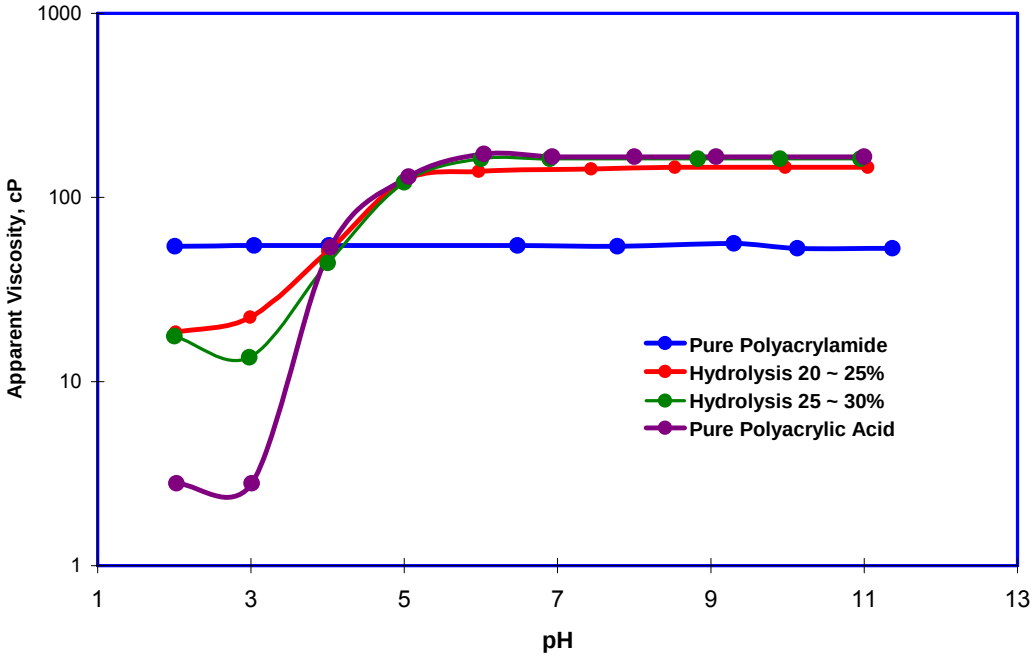

I.3. Future Work

The following work is planned to evaluate HPAM polymer in the application of novel mobility and conformance control:

- Laboratory measurements of viscosity of HPAM as a function of pH, degree of hydrolysis, polymer and salt concentration
- Development and evaluation of a rheological model of HPAM as a function of above variables.
- Core flood tests for HPAM propagation for transport evaluation.
- Development and evaluation transport model
- Core-level simulation
- Field-level simulation

Appendix II. Application of pH triggered polymers to increase sweep efficiency in fractured reservoirs

II.1. Introduction

One way to overcome the channeling problem is to block the high permeability zones with a specific kind of polymer or gel. By blocking the already swept areas, subsequently injected water can sweep the unswept area of the reservoir and increase the oil recovery. The polymer should be highly viscous in order to block the high permeability zones, and ideally these polymers should be economical and easy to prepare. To inject such a viscous polymer into the reservoir more powerful pumps must be used. However, one problem is that the fracture gradient is limited and the reservoir could be fractured if this limit is exceeded through the use of high pressure pumps. With this object, a non-viscous polymer which can be injected easily into the reservoir is needed. After injection this polymer should expand and swell, forming a highly viscous gel into the high permeability zones to seal the fractures successfully.

Research objectives

The research objectives of this Task are listed below:

1. Studying the applicability of using pH triggered polymers in order to block the high permeability zones and increase the sweep efficiency by doing several polymer injections into the fractured sandstone and fractured limestone cores
2. Finding the best pH triggered polymer among the available polymers, based on their chemical interaction with different rock mineralogy
3. Studying the polymer chemical and physical interaction with different rock minerals
4. Doing experiments on sandstone, limestone and igneous fractured and vuggy cores to fully understand the effect of different factors such as injected water salinity and polymer yield stress in this new application of pH triggered polymers
5. Conducting constant pressure water injection experiments in order to find the polymer yield stress
6. Finding a way to perform the experiments on cubic blocks of vuggy rocks more accurately.
7. Doing several experiments on the fractured cores which are made from Lucite in order to eliminate the matrix effect on polymer. Use the results to study the polymer yield stress and ability of the microgel to block the high permeability zones more accurately.
8. Simulating the water and polymer flow through the fractures, using commercial simulators such as ECLIPSE and CMG
9. Developing the theory of flowing the polymer into the fractured reservoirs according to the experimental results to explain the behavior of the pH triggered polymers in these kinds of reservoirs.

II.2. Method for conducting the research

II.2.1. Preparing the sandstone and limestone cores

All the cores were cut from homogenous blocks of Berea sandstone and Texas Cream chalk. The diameter of the cores was 1 inch and the length varied from 11.3 to 11.6 inches (Fig. 1). To make a fractured core, the core was cut in half along its length with a very thin rotating

saw. After that, the core was placed in the oven to evaporate the residual water in the pores, then coated with heat shrink Teflon which keeps both laps of the core tightly together. The core edges were not sealed with epoxy because this causes two problems: 1) applying the epoxy causes the core sides to be uneven and 2) epoxy may leak into the core and block the fracture.

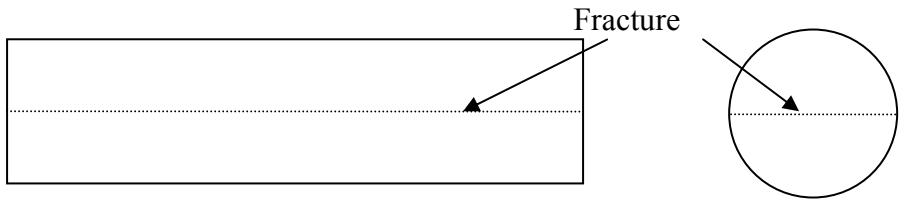

Fig. II.1: Side views of a fractured core

II.2.2. Preparing the polymer

The composition of the desired polymer is 94 % water, 3% NaCl, and 3% Carbopol® 934. The 3% brine was prepared first then the polymer was added, using a magnetic stirrer to mix the solution. After approximately one day, the polymer had dissolved in the brine completely. The stirrer was then set to a very low speed to get rid of air bubbles entrained during dissolution. After another day the polymer was examined under light. If air bubbles are visible, the polymer should be vacuumed before injection. Otherwise, the polymer is ready to use and may be injected directly into the core.

II.2.3. Experiments on sandstone and limestone cores

The fractured cores were placed in a horizontal Hassler core holder one-inch in diameter and one-foot in length. The pressure differences between the inlet and outlet of the core were measured using three pressure gauges which were set in parallel. The brine, acid and polymer were injected into the core using a piston pump that can be set to a constant injection rate of up to 10 cc / min.

After core saturation, the brine was injected into the core and the core's pressure drop was measured to calculate its primary permeability. In order to calculate the fracture aperture, the equation of flow in a wide open slit was used. Next, brine with different salinity was injected into the core and a tracer test was performed to see how fast the second brine would be produced from the core. Next, in some experiments the core was pre-flushed with 0.1M HCl to reduce the pH of the effluent at the core outlet to a desired value. Next, the polymer was injected into the core and the pump shut down. During the shut-in time, the effluent pH increased due to the reaction with the rock and to mixing with the connate water. This increase in effluent pH increased the viscosity of the microgel by 3 or 4 orders of magnitude. This caused the polymer to undergo the transition to gel and thus block the fracture. Next, brine was injected and the pressure drop measured to calculate the permeability after polymer gelation. Finally, brine with different salinity was injected to perform the tracer test after polymer gelation and compare it to the first tracer test.

All the experiments were done at constant injection rate. The next step was to conduct a series of injection experiments under constant pressure conditions to find out the yield stress of the polymer. After determining the polymer yield stress under different conditions, the

next objective was to find a way to increase the polymer yield stress to prevent the polymer from being pushed out by water due to high pressure water injection.

In future studies, more types of Carbopol polymers will be used, performing the polymer flood in a constant pressure process, trying to increase the yield stress of the polymer, simulating the flow through fractures using the commercial simulators, and finally examining the applicability of using pH triggered polymers to block the high permeability zones in different type of fractured and vuggy rocks.

II.2.4. Experiment on vuggy rock

The objective of this experiment was to study the possibility of blocking the connected pores in a block (7.5“by 2.5“by 2.5”) of vuggy basaltic rock using the Carbopol® 934. To do this experiment, a cell was constructed to hold the rock, then connected to a water container. Different pressure was applied to the rock through changes in the elevation of the container by up to 64 inches of water. After the initial core permeability was measured, the polymer (pH = 1.8) was injected into the cell using the piston pump. The pump was then shut-in and the cell sealed. According to previous batch experiments, it takes about 2 days for the pH of HCl acid contacted with the rock to change from 2 to 5 (Fig. 2) e.g. Batch experiment showed that the basaltic rock neutralizes weak HCl solution. After two days, the cell was reconnected to the water container and the first part was repeated in order to measure the reduced permeability and polymer yield stress.

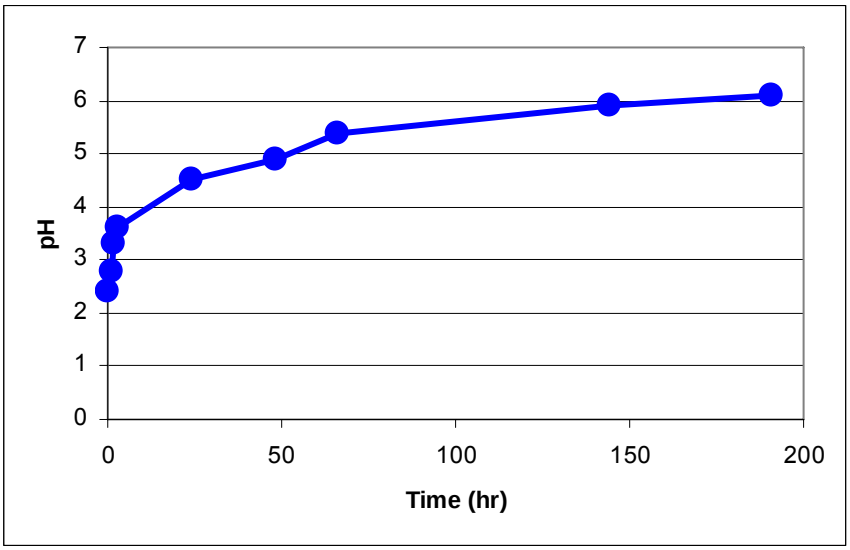

Fig. II.2: Changing pH of the HCl contacted with the basaltic rock

After the reduced permeability had been measured, the HCl 0.1M was injected into the cell to measure the ability of acid to restore the core to its original permeability. The cell was then filled with water and the polymer solution was injected again into the cell, which was then sealed for 2 days. The same experiment was then repeated using a water container to measure the core reduced permeability.

II.3. Preliminary results

As preliminary experiments, several polymer injection experiments were performed in fractured sandstone, fractured limestone and vuggy igneous cores. In fractured sandstone

cores the treatment reduced the permeability of the fractured cores by the factor of 2 to 230, depending on the length of the shut-in time. In fractured limestone cores polymer treatment reduced the permeability by a factor of 2. However, the axial and confining pressure on the core had to be relatively small because of the low strength of the limestone rocks. In addition, several tracer tests were performed using brine with different salinities. The results of tracer tests showed that the tracer comes out faster after gelation than before polymer gelation. This could be because of the water channeling through the gel or the open pore volume is reduced as a result of the treatment??

To summarize the results of the six experiments performed on fractured sandstone cores:

- Pressure drop across the core could be affected by the axial and confining pressures which have to be applied on the core. Confining pressure affects the aperture of the fracture, which affects the core permeability. The confining and axial should be kept constant in all experiments for the sake of consistency.
- By doing the polymer treatment, the initial permeability of the fractured cores (k_0) was reduced by the factor of 2 to 230 depending on the shut-in time. (Table 1)
- When brine was injected immediately after the polymer injection, the brine pushed out the polymer from the core resulting in a small permeability reduction (experiment #2).
- Acid pre-flush may not be needed in fractured reservoirs.
- It is preferable to use the compositional method to calculate the fracture permeability rather than $\frac{(fracture\,aperure)^2}{12}$. In compositional method, it can be assumed that the core is made of three parts: two matrix parts and one fracture, which are parallel with respect to the direction of flow. The values calculated by both methods differ in one order of magnitude.

***Table II.1*: Results obtained from polymer flood on fractured sandstone cores**

Experiment #	Initial permeability, md, k_0	Acid preflush	Polymer initial pH	Shut in Time	Reduced Permeability,md, k	k_0/k
1	4345	Yes	1.5	2 days	19	228.7
2	1697	Yes	2.2	10 minutes	952	1.8
3	2893	Yes	2.1	21 hours	148	19.5
4	2394	Yes	2.1	2 hours	535	4.5
5	2188	No	2	15 minutes	426	5.1
6	1238	No	2.1	2 hours	181.1	6.8

- The most important factor in using pH triggered polymers successfully in order to block fractures is gelation, or shut-in time (Fig. 3). However, the permeability reduction may also be slightly changed by an acid pre-flush.

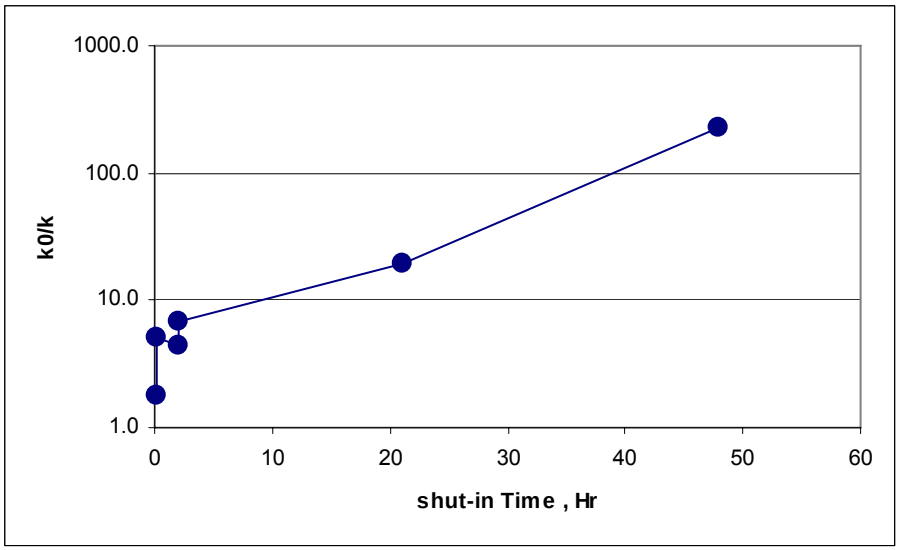

Fig. II.3: Permeability reduction versus shut-in (gelation) time in fractured sandstone cores

-
- Only 5 pore volume of acid is needed during the acid pre–flush in order to decrease the effluent pH down to 3 (Fig. 4), which is much less than the amount needed to decrease the effluent pH in un-fractured reservoirs (Choi, 2006).

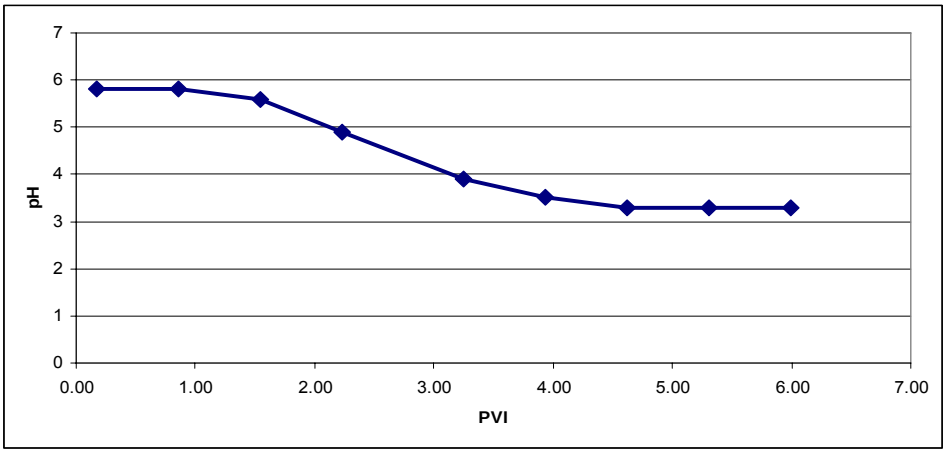

Fig. II.4: pH versus pore volume of injected acid into the core (experiment #3)

- The pressure drop across the core increased during polymer injection. This increase was not caused by gel formation but by the higher viscosity of the polymer with respect to the water viscosity.
- Two different brines with different salinities were used in order to do the tracer test. It was expected that after gelation and blocking of the fracture, the injected water would go to the matrix. Therefore, the tracer breakthrough time after gelation should have been larger than the tracer breakthrough time before gelation and should have showed a smooth S-shape curve. In almost all tracer tests (except #1), the tracer breakthrough occurred sooner and tracer curve is sharper after the polymer gelation if compared with the tracer

curve before polymer injection (Fig. 6). These results were not consistent with expectations. An explanation of these results has not yet been found, and more time will be needed to find a reasonable answer for this behavior. However, it may be because of the water channeling into the gel particles.

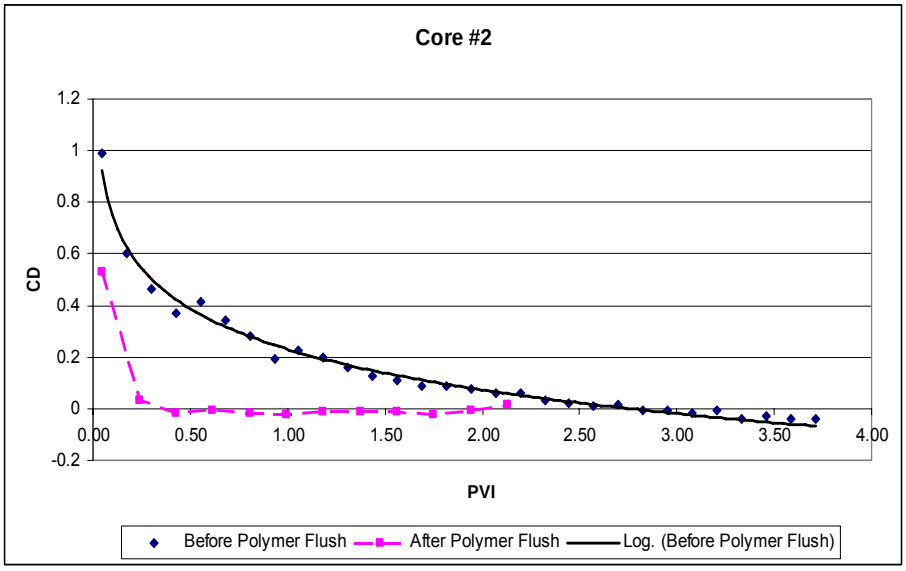

Fig. II.6: Tracer curves before and after polymer injection for experiment #2

Two experiments on fractured limestone revealed unexpected results. To perform the experiment on fractured limestone cores, the confining pressure was set to about 200 psi due to the low strength of fractured limestone cores. In this case, the treatment decreased the core permeability from 630 md down to 354 md after 2 hours of shut-in time. The pressure drop before and after polymer injection are shown in Fig.7. These results could be suspect because of the low confining pressure which let the injected water bypass the core and flow around the core all the way to the outlet. In the next experiments on limestone cores, shorter limestone cores will be used and the injection rate decreased in order to decrease the pressure drop across the core and make sure the water does not by-pass the core.

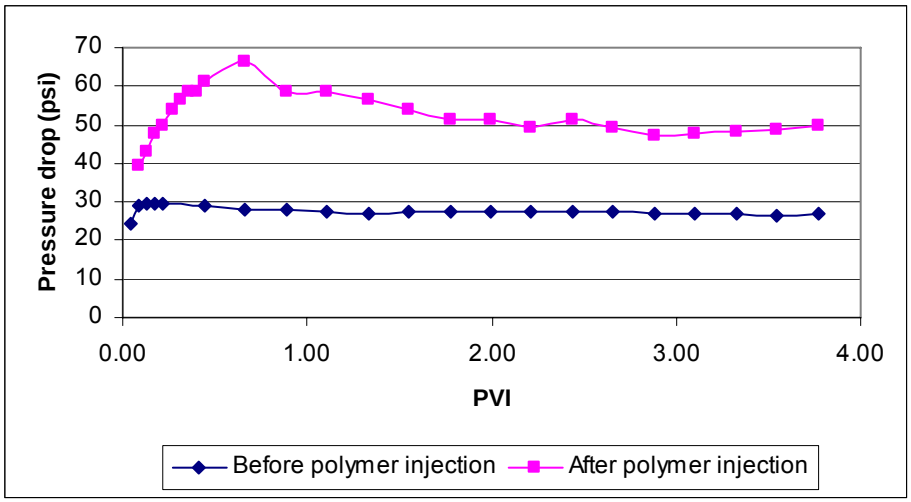

Fig. II.7: Pressure drop across the fractured limestone core before and after the polymer injection

Experiments on a vuggy igneous rock revealed the following results:

Acid injection can not restore the core to its original permeability

- In order to have a successful polymer treatment, the polymer solution should flow through the vugs
- The polymer solution did not mix with water in the cell and lay on the top of the core
- Two days after the second polymer injection, a solid microgel cake appeared on top of the core
- At a certain pressure, the water channeled through the polymer cake in three points (Fig 8)
- The polymer works as an on-off switch. As long as the microgel is in the vugs there is no flow across the core. Once the water pushes out the microgel, the flowrate returns to its previous value (Fig. 8).
-

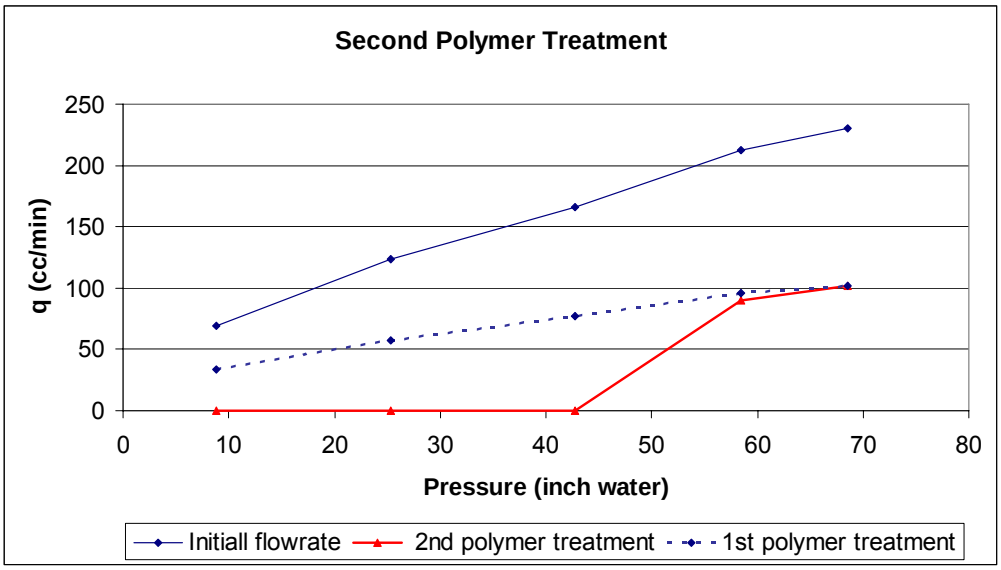

Fig. II.8: Water flowrate versus pressure from an experiment on a basaltic vuggy core

Appendix III

GEM-GHG Reservoir Simulator Description and

pH Sensitive Polymer Rheology Routine

The GEM – GHG simulator with pH sensitive polymer (PLM) capabilities was used because it is a compositional simulator that models geochemical reactions and the rheological behavior of pH sensitive polymer. This chapter is divided into two sections. The first section describes the Computer Modeling Group's GEM simulator with additional green house gas (GHG) geochemical reaction capabilities. The second section describes the additional viscosity routine implemented in the simulator that models the rheology of pH sensitive polymer.

III.1 DESCRIPTION OF THE GEM-GHG SIMULATOR

GEM, or Generalized Equation of State Model, is a compositional reservoir simulator that can perform multidimensional simulations. It can model three-phase multi-component fluid flow in petroleum reservoirs. GEM solves fluid flow calculations using implicit, explicit or adaptive implicit (implicit in some cells and explicit in the others) calculations. Separate fluid parameters are required for the aqueous and hydrocarbon phases. The GHG program included in the version of GEM used for this project allows intra-aqueous reactions and geochemical reactions between minerals and aqueous species. The chemical reactions are determined by user-defined stoichiometric reactions. This code was developed to model the sequestration of carbon dioxide and the subsequent reactions between dissolved minerals and ions in solution and the ionized carbon dioxide.

GEM-GHG Fundamental Transport Equations

The reservoir simulator solves transport equations for each species in the model using fundamental transport equations.

For hydrocarbon species:

$$\phi \frac{\partial C_i}{\partial t} + u \vec{\nabla} \cdot C_i = r_i \qquad \text{[III.1]}$$

where C_i is the concentration of species i, t is time, r_i is the rate of transfer of I (r_i is 0 except when Henry's law constant is used), and u_i is the Darcy velocity of species i

For aqueous species:

$$\phi \frac{\partial C_i}{\partial t} + u \vec{\nabla} \cdot C_i = R_i + r_i + K_i \vec{\nabla} \cdot \left[\vec{\nabla} \cdot C_i \right] \qquad \text{[III.2]}$$

where R_i is the reaction rate of species i and r_i is the rate of transfer from the hydrocarbon phase, K_i is the dispersion coefficient of species i.

For rock mineral species:

$$\phi \frac{\partial C_i}{\partial t} = -R_i \qquad \text{[III.3]}$$

Henry's Law

When a gaseous species is soluble in the aqueous phase the species may enter the geochemical reactions in the reservoir. This is the case when carbon dioxide (CO_2) is present in the reservoir. The gaseous and aqueous species are in equilibrium with the equilibrium constant being estimated by Henry's Law, which can be represented as:

$$CO_{2(g)} = CO_{2(aq)} \qquad \text{[III.4]}$$

GEM uses Henry's law to calculate the solubility of a soluble gas. Henry's law states that the concentration of the dissolved gas species is proportional to the partial pressure p_i of that species in the gas phase.

$$x = f_i / H_i \qquad \text{[III.5]}$$

where f is the fugacity of the component, x is the concentration of the component in the aqueous phase, and H is the Henry's law constant

GEM calculates the Henry's law constant as follows:

$$H = \exp [\ln (henry) + v_\infty * (p-P_0)/RT] \qquad \text{[III.6]}$$

where henry is the reference Henry's law constant of the component at a reference pressure (kPa), P_0 is the reference pressure for the given Henry's law constant (kPa), v_∞ is partial molar volume of the component in water at infinite dilution (liter/mol), R is universal gas constant (8.314 J/(mol * K)), and T is temperature (K)

Chemical Reactions

GEM is capable of modeling chemical reactions using two methods. The first method is to model homogeneous chemical reactions in the aqueous phase as those that achieve equilibrium instantaneously. The second method is to model mineral dissolution or precipitation reactions with aqueous ions as rate controlled reactions.

The stoichiometric coefficients (ν_k) for any reaction must satisfy the requirement:

$$\sum_{k=1}^{n_s} \nu_k A_k = 0 \qquad \text{[III.7]}$$

where A_k is the species name, k is the species number, and n_s is the total number of species present in the simulation. In GEM, no minerals may be involved in the intra-aqueous equilibrium reactions, and only one mineral component A_k may be present in a rate controlled reaction.

Intra-aqueous Equilibrium Reactions

A chemical reaction is in equilibrium if the forward reaction rate and backward reaction rates are equal giving a net reaction rate of zero. GEM models reactions between ionic species in the aqueous phase as equilibrium reactions.

Reactions in equilibrium satisfy the following condition:

$$Q - K_{eq} = 0 \qquad \text{[III.8]}$$

$$\text{where } K_{eq} = \exp\left[-\frac{1}{RT} * \sum_{k=1}^{n_s} \nu_k \left(\Delta G_f^0\right)_k\right] \qquad \text{[III.9]}$$

$$\text{and } Q = \prod_{k=1}^{n_s} (a_k)^{\nu_k} = \text{activity product of reaction} \qquad \text{[III.10]}$$

Activities for each species (a_k) are related to their concentration in solution. The activities of water and the mineral species can be taken to be unity without introducing significant errors Helgeson *et al.*, 1970). Activities in ideal cases can be taken to be approximately equal to the concentration of the species in molality. The Debye-Huckel or B-dot methods to calculate activities can be used in GEM although they were not used in any simulations since the "ideal" activity method was selected.

Modeling intra-aqueous reactions as instantaneous equilibrium reactions neglects their actual reaction times, but this simplification allows increased computational efficiency by permitting the use of an equilibrium-rate-annihilation (ERA) matrix to be used to reduce the number of flow equations (Nghiem, 2002). Neglecting the reaction rates of intra-aqueous reactions is reasonable assuming that mineral reactions control the net reaction rates in the brine.

Defining equilibrium reactions in GEM is done by defining the number of equilibrium reactions with the *N-CHEM-EQUIL keyword, defining whether numerical or analytical rate derivatives should be used, and by defining the stoichiometric coefficients for each reaction using the *STOICHIOMETRY keyword

The equilibrium reactions modeled in the history match simulations are given below. These values were taken from Stumm and Morgan (1996). Table 4-2 gives a reduced set of reactions that was used for the pH sensitive polymer simulations. Intra-aqueous reactions that include species not present in the reservoir minerals should not be included in a simulation.

The log K_{eq} values for each reaction change as a function of temperature. Instead of entering a single log K_{eq} value for each reaction, the user may choose to enter a, b, c, d, and e coefficients so that GEM can calculate log K_{eq} as a function of temperature (ºC).

$$\text{Log } K_{eq} = a + b\,(T)^1 + c\,(T)^2 + d\,(T)^3 + e\,(T)^4 \qquad \text{[III.11]}$$

Table III-1: Intra-aqueous Reactions Equilibrium Constant Values Used in Numerical Simulations

Equilibrium Reaction	Log Keq @ 25ºC
$HCO_3^- = H^+ + CO_3^{--}$	-10.329
$Al^{+++} + 4\ H_2O = Al(OH)_4^- + 4\ H^+$	-22.7
$H_2CO_3 = 2\ H^+ + CO_3^-$	16.6
$H_2O = H^+ + OH^-$	-14
$Mg^{++} + CO_3^{--} = MgCO_{3(aq)}$	2.98
$Mg^{++} + HCO_3^- = MgHCO_3^+$	1.07
$Mg^{++} + H_2O = MgOH^+ + H^+$	-11.44
$Na^+ + H_2O = NaOH_{(aq)} + H^+$	-14.18
$K^+ + H_2O = KOH_{(aq)} + H^+$	-14.46
$Na^+ + CO_3^{--} = NaCO_3^-$	1.27
$Na^+ + HCO_3^- = NaHCO_{3(aq)}$	-0.25
$Ca^{++} + CO_3^{--} = CaCO_{3(aq)}$	3.224
$Ca^{++} + HCO_3^- = CaHCO_3^+$	1.106
$Ca^{++} + H_2O = CaOH^+ + H^+$	-12.78
$Al^{+++} + H_2O = AlOH^{++} + H^+$	-5.00
$Al^{+++} + 2\ H_2O = Al(OH)_2^+ + 2\ H^+$	-10.1
$H_4SiO_4 = H_3SiO_4- + H^+$	-9.83
$H_4SiO_4 = H_2SiO_4^{--} + 2\ H^+$	-23.0

Rate Controlled Reactions

Reactions between the aqueous species and the reactive minerals in a reservoir are kinetically controlled. Reactions involving reservoir minerals cause minerals to dissolve or precipitate when they are not in a state of equilibrium.

Mineral reactions in GEM must be written so the mineral has a stoichiometric coefficient of -1, and so there is only one mineral involved per reaction. The dissolution or precipitation rate of a mineral is calculated as:

$$r_\beta = \mathrm{sgn}\left[1-\left(\frac{Q_\beta}{K_{eq,\beta}}\right)\right]\hat{A}_\beta S_w\left(k_{0,\beta}+\sum_{i=1}^{n_{aq}} k_{i,\beta} a_i^{\omega_{i,\beta}}\right)\left|1-\left(\frac{Q_\beta}{K_{eq,\beta}}\right)^{\xi_\beta}\right|^{\varsigma_\beta}, \beta = 1\ldots R_{mn} \qquad \text{[III.12]}$$

where:

$\hat{A}_\beta$ = reactive surface area of reactant mineral β per unit bulk volume of porous medium (m^2/m^3)
S_w = water saturation

$k_{0,\beta}$ = rate constant of mineral reaction β (mol/m^2·s)
$k_{i,\beta}$ = rate constants of mineral reaction β related to activity (default = 0 in GEM)
$a_i^{\omega,\beta i}$ = activity of ions for mineral reaction β
$K_{eq,\beta}$ = chemical equilibrium constant of mineral dissolution/precipitation reaction
Q_β = activity product of mineral β dissolution reaction
r_β = dissolution/precipitation rate per unit bulk volume of porous medium [mol/(m^3·s)]
R_{mn} = number of mineral reactions
ξ_β = parameter (default = 1 in GEM)
ζ_β = parameter (default = 1 in GEM)

The sgn (signum) function returns the sign of the expression in brackets. A positive sign for this equation indicates the reaction is a dissolution reaction; a negative sign indicates a precipitation reaction.

Reaction rates are normally stated at a reference temperature. The rate constant (k) at any desired temperature can be found using the following equation:

$$k_\beta = k_{0,\beta} \exp\left[-\frac{E_a}{R}\left(\frac{1}{T}-\frac{1}{T_o}\right)\right] \qquad \text{[III.13]}$$

Where, E_a = activation energy for reaction (J/mol), $k_{0,\beta}$ = reaction rate constant for reaction at reference temperature, R = universal gas constant (8.314 J/(mol K)), T = temperature (K) and T_0 = reference temperature (K)

The reactive surface area of mineral per unit bulk volume of porous medium changes as the mineral dissolves or precipitates. GEM employs the following equation to adjust the reactive surface area:

$$\hat{A} = \hat{A}_0 \cdot \frac{N_\beta}{N_{\beta 0}} \qquad \text{[III.14]}$$

Where, $\hat{A}_0$ = reactive surface area at time zero, N_β = moles of mineral β per grid block volume at current time, and $N_{\beta 0}$ = moles of mineral β per grid block volume at time zero

The porosity of the matrix changes as minerals are dissolved or precipitated. GEM calculates the effective porosity of each grid block using the following

$$\phi_{eff} = \phi + \sum_{\beta=1}^{n_{mn}}\left(\frac{N_\beta}{\rho_\beta} - \frac{N_{\beta 0}}{\rho_\beta}\right) \qquad \text{[III.15]}$$

Where, n_{mn} = number of reactive minerals present in simulation, N_β = total moles of mineral β per bulk volume, $N_{\beta 0}$ = total moles of mineral β per bulk volume initially present, ρ_β = density of mineral β, and ϕ is the porosity calculated as a function of pressure based on:

$$\phi = \phi^* \left[1 + c_\phi (p - p^*) \right] \qquad \text{[III.16]}$$

Where, ϕ^* = porosity value at reference pressure p^*, and c_ϕ = rock compressibility (kpa^{-1})

Permeability changes as the porosity changes. This effect is modeled in GEM using the Kozemy-Carman equation:

$$k = k_0 \left(\frac{\phi_{eff}}{\phi_{eff}^0} \right)^3 \left(\frac{1 - \phi_{eff}^0}{1 - \phi_{eff}} \right)^2 \qquad \text{[III.17]}$$

where k = effective permeability, and k_0 = initial effective permeability

3.2 pH Sensitive Polymer Rheology Model

The polymer code in GEM-GHG-PLM allows the calculation of pH sensitive polymer solution viscosity based on the rheological model developed by Huh, Choi and Sharma (2005). Lalehrokh and Choi developed Fortran code to calculate the viscosity of pH sensitive polymer which was then implemented in the GEM code by the Computer Modeling Group. Polymer viscosity in the simulator is controlled by user-defined polymer properties and by the polymer concentration, aqueous phase pH and ionic strength, and the shear rate of the fluid in the simulation run. The remainder of this section contains a detailed description of how GEM calculates pH sensitive polymer viscosity and charts showing pH sensitive polymer solution viscosity as a function of pH, in situ fluid velocity, ionic strength and polymer concentration.

The following description of the pH sensitive polymer viscosity calculations is taken from "A Rheological Model for pH Sensitive Ionic Polymer Solution" (Choi et al., 2006). GEM follows the steps shown below in Figure 3.2.1 to calculate the polymer viscosity for each time step. The input for the polymer viscosity program comes from the GEM input file and internally from data calculated within GEM.

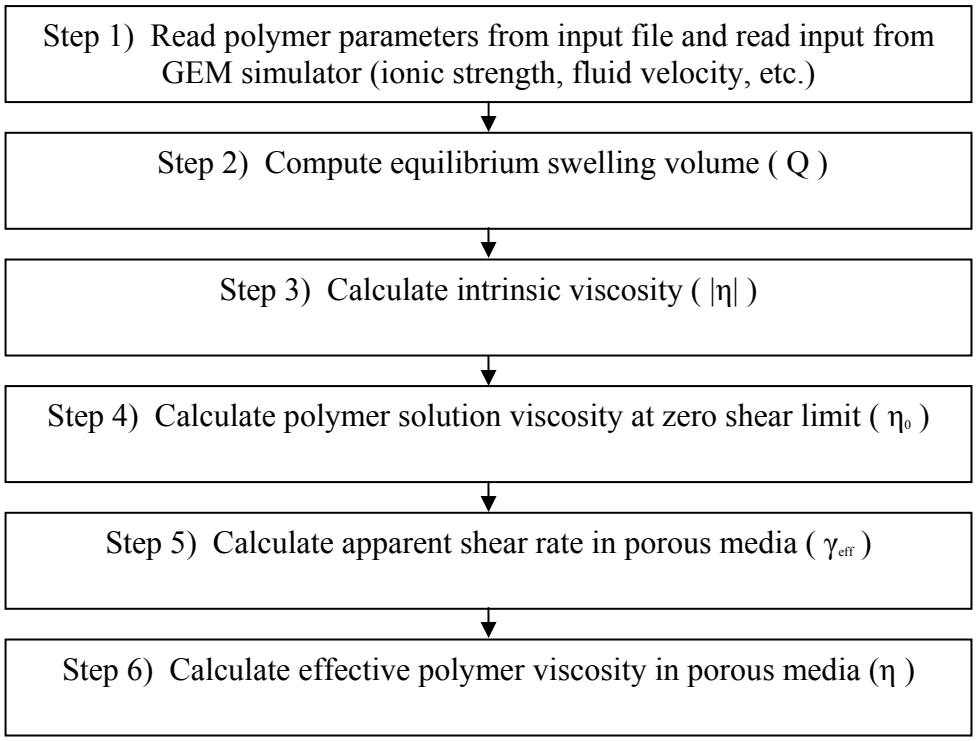

Figure III-1: Viscosity Code Calculations Flow Chart

Table III-2: Internal GEM Polymer Viscosity Code Variables

Variable	Units
Polymer volume fraction in the swollen network , $\upsilon_{2,s}$	None
Equilibrium swelling volume, Q	None
Polymer intrinsic viscosity, $\lvert\eta\rvert$	None
Polymer solution viscosity in the zero-shear-limit, η_o	cp
Effective polymer shear rate in cell, γ_{eff}	s^{-1}
Carreau equation empirical parameter, n	None
Carreau equation empirical parameter, λ	None
Ionic strength of polymer solution, I	None
pH of polymer solution, pH	None

Polymer Viscosity Comparison

A comparison between the viscosity values calculated from the pH sensitive polymer rheological model (implemented in a spreadsheet calculation by Choi) and the GEM simulator was performed to ensure they matched. GEM simulation runs based on polymer

concentration, polymer pH, polymer velocity and solution ionic strength showed excellent agreement between the two codes. The relative error in the viscosity values was less than 1% for all cases except at high fluid velocity rates (which causes high shear rates.) For the high velocity cases inspection of the viscosity versus polymer velocity data showed that the absolute differences in viscosity remained small despite the viscosity being several orders of magnitude smaller than the zero shear values.

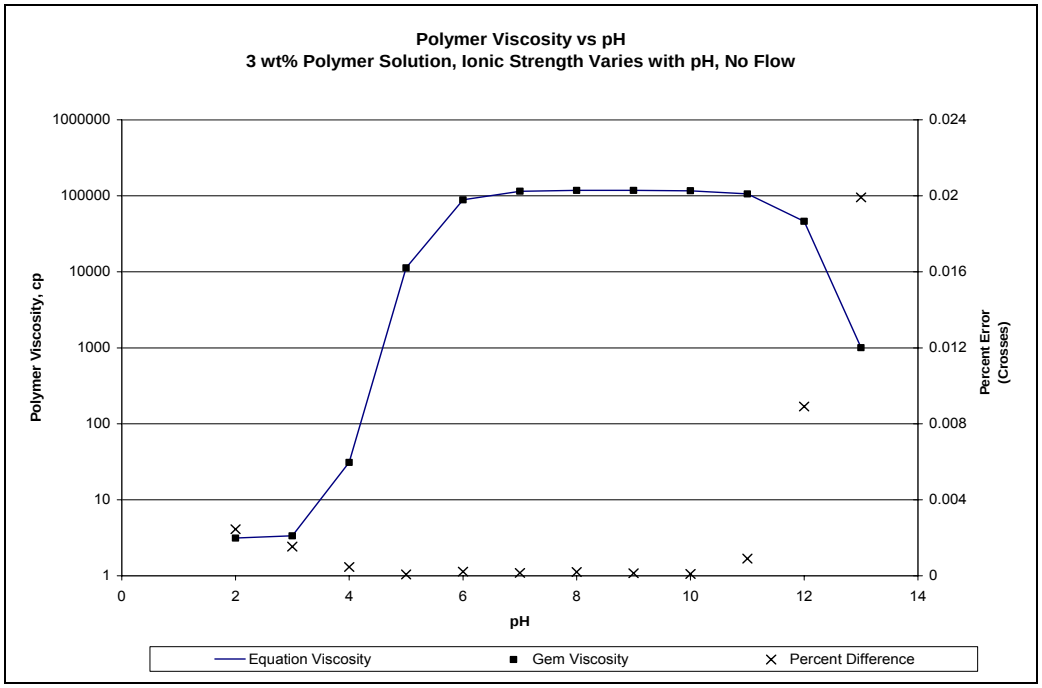

Figure III-2: Polymer viscosity versus pH of 3 wt % polymer solution

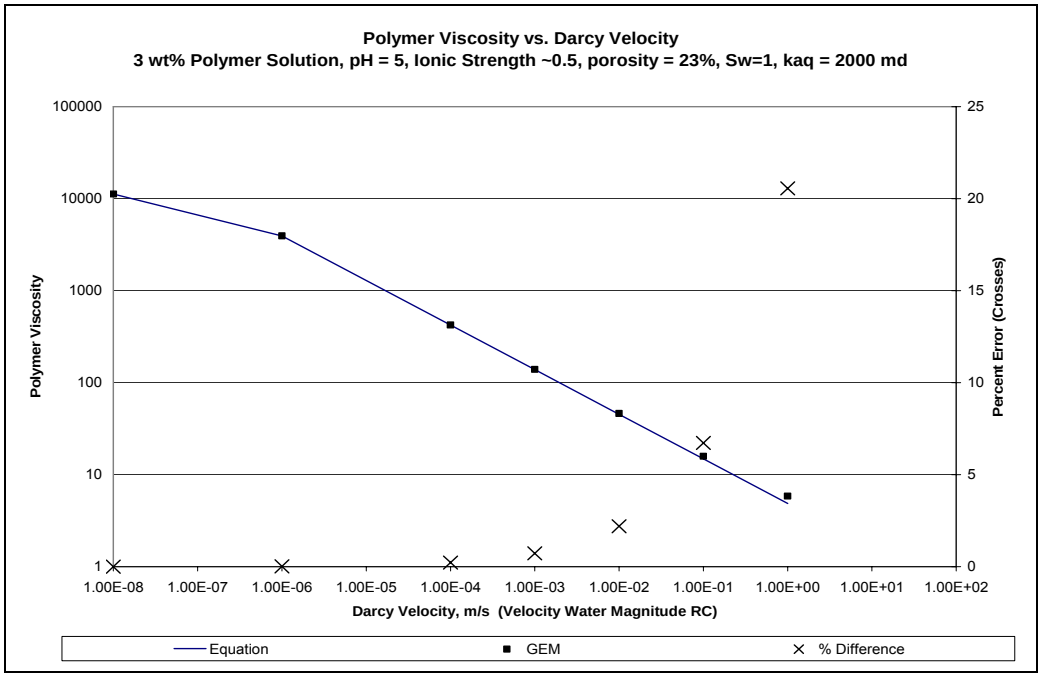

Figure III-3: Polymer viscosity versus fluid velocity

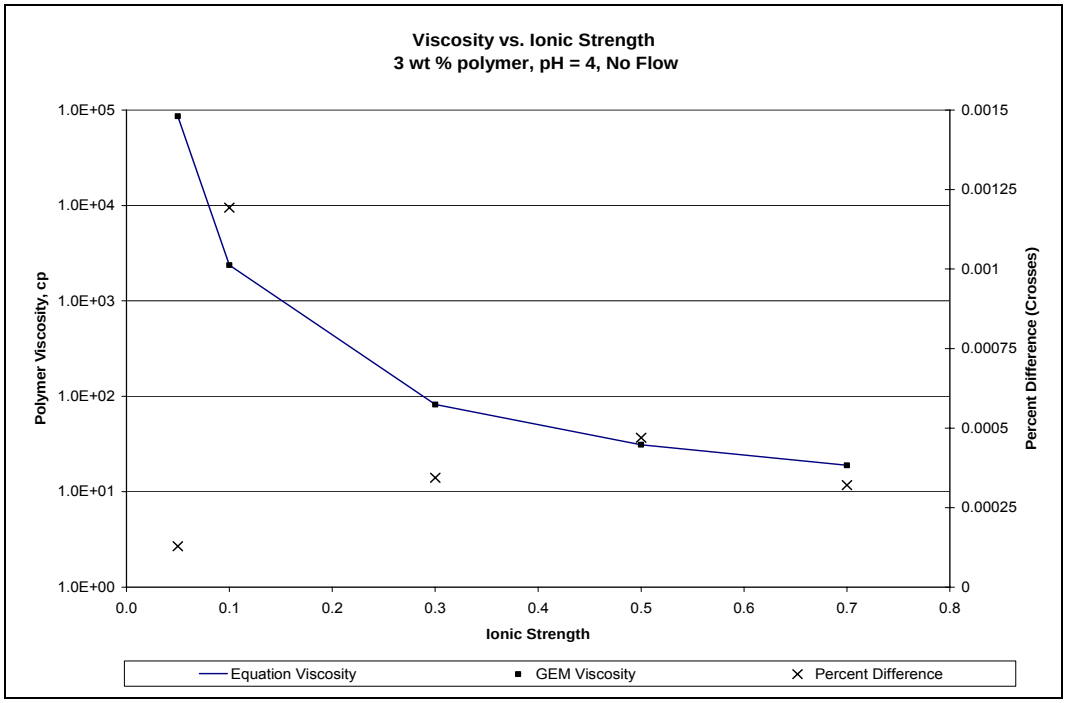

Figure III-4: Polymer viscosity versus ionic concentration

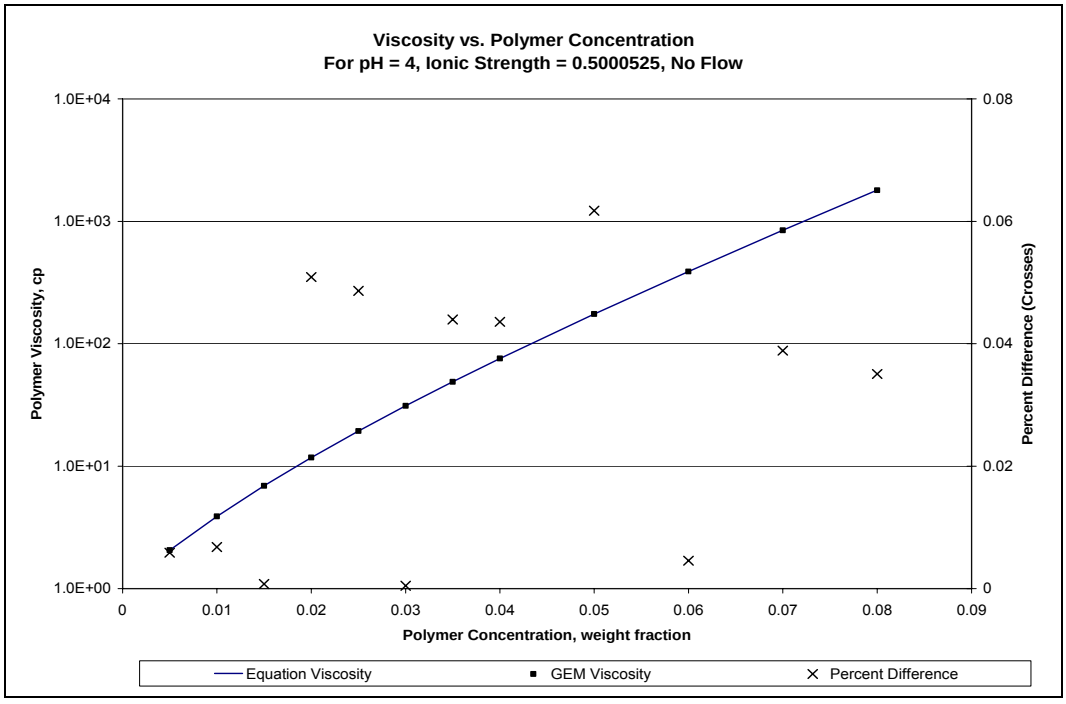

Figure III-5: Polymer viscosity versus polymer concentration

Appendix IV
Characterization of Reservoir–Brine Interactions Using Geochemical Simulations

Reservoir minerals may react with injected brine solutions to alter the composition and pH of the brine. Such brine-mineral reactions must be accurately characterized to model the behavior of pH sensitive polymer in situ. This chapter documents the results of the history matching procedure used to model the reaction of hydrochloric acid with Berea sandstone. Three Berea core flood experiments conducted by Choi served as the basis for this work. The GEM-GHG simulator was used to model the core floods. The chosen final mineralogy and reaction parameters matched the pH behavior of the core flood effluent reasonably well. This chapter concludes with a discussion of the chosen Berea core mineralogy and reaction coefficients in regards to the history matching process.

Berea Core Floods

Choi (2005) performed three core flood experiments with Berea sandstone cores to estimate the pH inside Berea sandstone while it is being flooded with acid. A solution of 3 wt % NaCl brine was injected at the start of these core floods, followed by injection of hydrochloric acid with a pH of 1. The experiments were carried out at a temperature of 24°C. The rate of fluid injection was varied in the first and third core flood experiment, and the rate was held constant for the second experiment. Shut in periods occurred during the experiments by design or to allow refilling of the injection pump. Nearly continuous effluent pH readings were taken for all three experiments. Additional silicon, aluminum, calcium, iron and potassium concentrations were measured in effluent samples taken during the second experiment. The core dimensions and porosities for the experimental cores are given below. Other information can be obtained from "A Study of a pH-Sensitive Polymer for Novel Conformance Control Applications" (Choi, 2005).

Table IV-1 Core Dimensions and Properties

Experiment	Core Length	Core Diameter	Core Porosity
Core Flood 1	0.2247 m	0.0249 m approx.	0.20
Core Flood 2	0.2247 m	0.0249 m	0.177
Core Flood 3	0.2247 m	0.0248 m	0.1825

Note: The core diameter recorded by Choi was 1 inch but has been approximated as 0.0249 m in the simulations since the other two "1 inch" diameter cores had a smaller diameter.

Typical Berea Mineralogy

Ermel (2005) summarized Berea compositions given in the literature which generally include a large proportion of quartz with small proportions of carbonate, feldspars, and clays (illite, smectite, chlorite, kaolinite). Ermel's work to match the same three core floods performed by Choi identified that including Anorthite in a simulation can provide a good match of the observed pH values. The following minerals were included in the current attempts to history

match the pH effluent behavior exhibited by the core floods: quartz, kaolinite, anorthite, calcite, potassium feldspar and illite.

History Matching Procedure

Initial attempts were made by the author to recreate the successful history match that Ermel achieved using the KGEOFLOW simulator for the second core flood with kaolinite and anorthite representing the Berea core. This attempt failed using the GEM simulator because the anorthite spontaneously converted to kaolinite except at very high pH values.

A more methodical approach was taken to model the Berea sandstone using commonly identified constituent minerals by taking the following steps:

1) Identify minerals that were likely to be present in Berea sandstone based on literature search. In this case quartz, kaolinite, calcite, potassium feldspar and illite were selected.

2) Select a primary matching parameter. Matching the observed effluent pH of ~5 when pH 1 hydrochloric acid was being injected into the Berea cores was selected as the primary matching parameter.

3) Perform simulations to identify the equilibrium pH values achieved between pH 1 HCl acid and single minerals and groups of mineral. Equilibrium pH values are the final pH values that a brine-mineral system will attain given infinite time. This was approximated in GEM by injecting acid into a core containing the desired minerals while increasing the mineral reaction rates or core length to achieve a very large Damkohler number. The equilibrium pH and ion concentrations were identified when the spent acid composition no longer changed with distance traveled in the core. Mineral combinations that did not raise the pH of the acid to 5 of above were unacceptable representations for Berea.

4) Evaluated model results. Initially a pH of 5 could not be obtained from the calcite reaction which did not seem correct. Additional aqueous phase reactions and ionic species (such as H_2CO_3) were then added. A sample case was run to compare the calcite reaction described a GEM test file with an example from page 375 of Aquatic Chemistry (Stumm and Morgan, 1996) to ensure that the simulated calcite reactions were correct. New equilibrium pH values (step 3) were calculated with the new aqueous species reactions.

5) Calcite was considered the prime reactive mineral since it reacted with pH 1 acid to given an effluent pH of ~5.4 which was close to the observed effluent pH of ~5. Simulations with calcite combined with quartz and/or potassium feldspar had a similar equilibrium pH.

6) It was recognized that adding anorthite, kaolinite or illite to quartz and potassium feldspar drive the equilibrium pH above 6 in the core. It was desired to have a final pH greater than six or seven to test the concept of pH sensitive polymer gelling to very high viscosities. The likely combination of kaolinite, calcite, quartz and potassium feldspar was chosen for further matching since it closely matches the Berea sandstone composition most often cited in literature.

7) Analysis of the calcite, kaolinite, calcite, potassium feldspar model revealed that many of the intra-aqueous reaction equations could be removed from the simulation without materially changing the effluent pH or metal ion concentrations. Only the significant interaqueous reactions, namely the dissociation of H_2O, H_2CO_3, $Al(OH)_4^-$ and HCO_3^- (see Table 4-2), were left in the simulation model before further matching efforts were undertaken to shorten the simulation run times.

Table IV-2 Intra-aqueous Reactions Equilibrium Constants for Final Match Simulations

Equilibrium Reaction	Log Keq @ 25ºC
$HCO_3^- = H^+ + CO_3^{--}$	-10.329
$Al^{+++} + 4\ H_2O = Al(OH)_4^- + 4\ H^+$	-22.7
$H_2CO_3 = 2\ H^+ + CO_3^-$	16.6
$H_2O = H^+ + OH^-$	-14

8) A run using an average Berea composition, and published reaction rate constants compiled by Xu, Apps and Pruess (2001) revealed that the minerals did not react fast enough to raise the pH of 0.1 M HCl much given the core properties and flow rates of the second core flood experiment. The mineral reaction rates and the calcite volume fraction were adjusted to give a reasonable match for the effluent pH and ion concentrations for the second core flood.
9) The chosen mineralogy and reaction rates, called the "initial match" parameters and volume fractions determined for experiment two were used to simulate core flood experiments one and three. It was found necessary to increase the calcite reaction rate to prevent the simulated effluent pH from dropping during the higher acid injection rates in experiment three. The quartz, kaolinite and potassium feldspar reaction rates were decreases to match the number of pore volumes of pH 1 acid that had to be injected before the effluent pH from the core flood dropped from about 5 to about 1.5. The resulting "final match" core mineralogy is given in Table IV-5 and reaction parameters are given in Tables IV-3 and Table IV-4.

Simulation Input

The following table gives the mineral reactions and associated equilibrium constants used during the history matching process. All the simulations were run using values at 25°C.

Table IV-3 Mineral Reactions and Equilibrium Constants (at 25°C)

Mineral	Reaction	log K_{eq}
Quartz	$SiO_{2(s)} + 2\ H_2O = H_4SiO_{2(aq)}$	-3.98
Kaolinite	$Al_2Si_2O_5(OH)_{4(s)} + 6\ H^+_{(aq)} =$ $2\ Al_3^+{}_{(aq)} + 2\ H_4SiO_{4(aq)} + H_2O$	7.435
Calcite	$CaCO_{3(s)} = Ca^{2+}_{(aq)} + CO_3^{--}{}_{(aq)}$	-8.42
Potassium feldspar	$KAlSi_3O_{8(s)} + 8\ H_2O =$ $K^+_{(aq)} + Al(OH)_4^-{}_{(aq)} + 3\ H_4SiO_{4(aq)}$	-20.573
Illite	$K_{0.6}Mg_{0.25}Al_{2.3}Si_{3.5}O_{10}(OH)_{2(s)} + 8\ H^+_{(aq)} + 2\ H_2O = 0.6$ $K^+_{(aq)} + 0.25\ Mg^{2+}_{(aq)} + 2.3\ Al^{3+}_{(aq)} + 3.5\ H_4SiO_{4(aq)}$	9.8
Anorthite	$CaAl_2Si_2O_{8(s)} + 8\ H^+_{(aq)} = Ca^{2+} + 2\ Al^{3+} + 2\ H_4SiO_{4(aq)}$	21.81

Table IV-4 contains mineral reaction constants (in moles m^{-2} s^{-1}) from Xu *et al.* (2001) and from the history matching exercise.

Table IV-4 Mineral Reaction Constants (at 25°C)

from Literature and History Matching

Mineral Reaction	Log k – *Xu et al.*	Log k – initial match	Log k – final match
Quartz	-13.9	-6.22	-6.52
Kaolinite	-13.0	-7.2	-7.5
Calcite	-8.8	-4.07	-3.37
Potassium feldspar	-12.0	-5.98	-6.28

The mineral compositions, initial reactive surface areas and activation energies are given in Table IV-5. The compositions given in the Table IV-5 are given as a fraction of grain volume and must sum to one. They must be multiplied by (1-porosity) which gives the compositions in terms of volume fraction before they are entered into the GEM-GHG input file. The specific reactive areas given in the table are defined similarly to Xu *et al.* (2001).

Table IV-5 Mineral compositions, Reactive Areas, and Activation Energies

Mineral Reaction	Simulated Composition	Specific Reactive Area (m2/[m3 of Bulk Volume])	Activation Energy (J/mol)
Quartz	0.846	10000 * Volume Fraction	87500.0
Kaolinite	0.061	1000000 * Volume Fraction	62760.0
Calcite	0.057	10000 * Volume Fraction	41870.0
Potassium feldspar	0.036	10000 * Volume Fraction	67830.0

Comparison of Experimental and Simulated Effluent Concentrations

Comparison of the effluent hydrogen (pH) and other measured cation concentrations between the simulation runs and the experimental observations served as the basis for selecting the mineralogy and reaction rates required to describe the acid-mineral reactions between berea sandstone and acid. Primary importance was placed on matching the pH of the effluent since the ultimate goal of this work is to model the behavior of pH sensitive polymer in sandstone reservoirs. Secondary importance was placed on matching the presence of certain cations, and tertiary importance was placed on matching the actual observed cation concentrations.

The simulation results presented do not include any shut in time although the experimental results include shut in time. Simulation of shut in time caused excessively high pressures to be generated in the model despite water and pore compressibility being included. GEM-GHG does not output ion concentrations at the producer wells so the ion concentration in the effluent side grid cell were plotted as the effluent concentrations.

Figures IV-1, IV-2 and IV-3 show the effluent pH vs. pore volumes of fluid injected for the first, second and third core flood experiments, respectively.

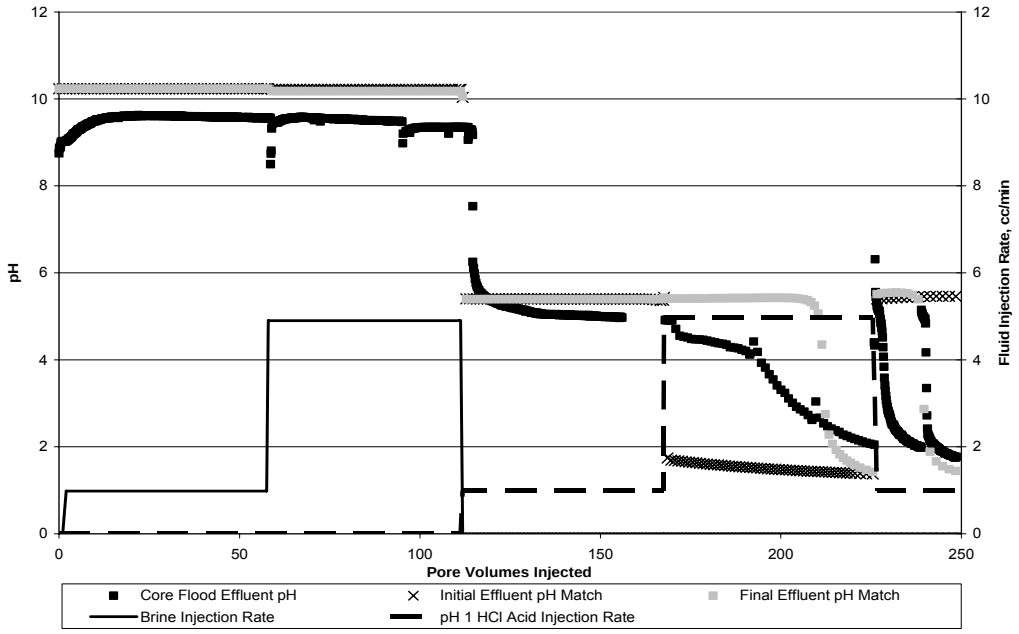

Figure IV-1: Effluent pH vs. Pore Volumes of Fluid Injected for First Core Flood

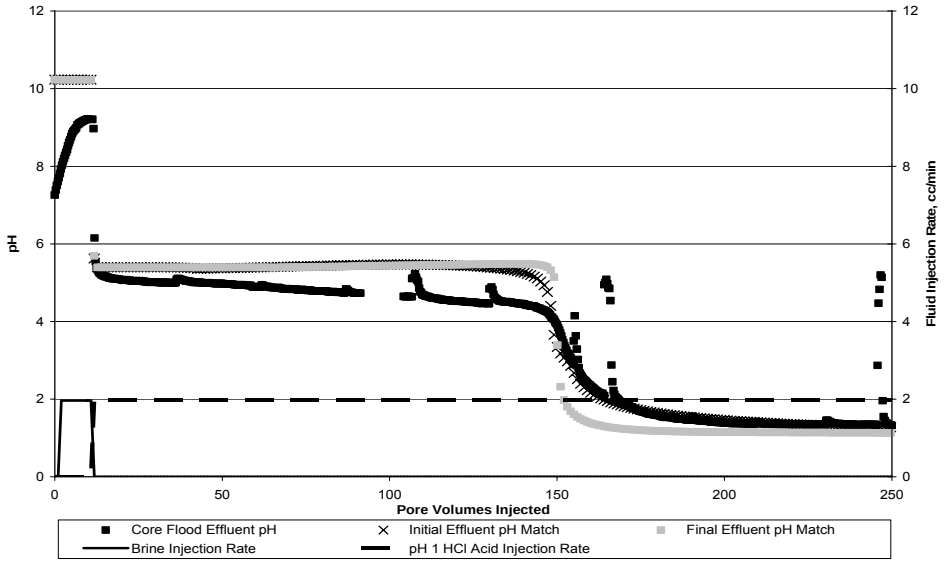

Figure IV-2: Effluent pH vs. Pore Volumes of Fluid Injected for Second Core Flood

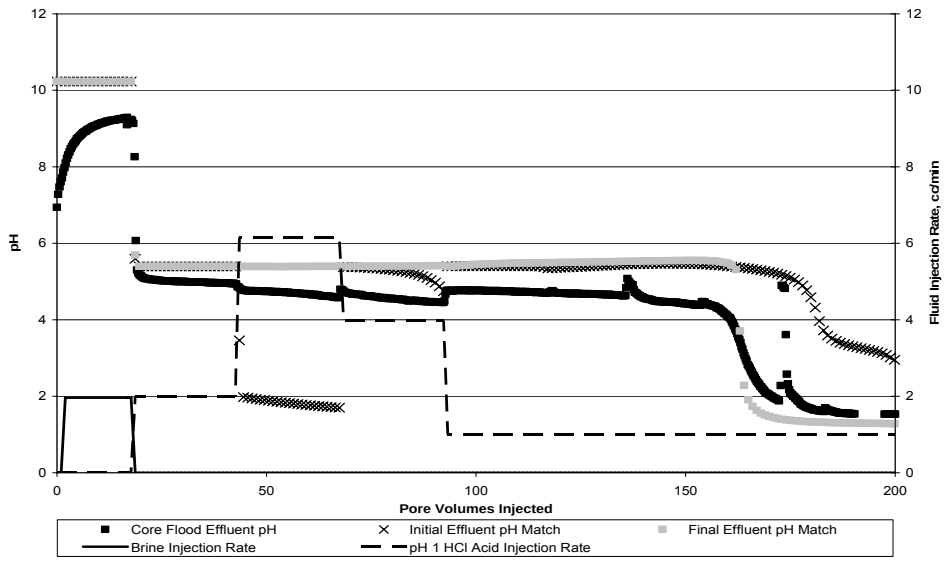

Figure IV-3: Effluent pH vs. Pore Volumes of Fluid Injected for Third Core Flood

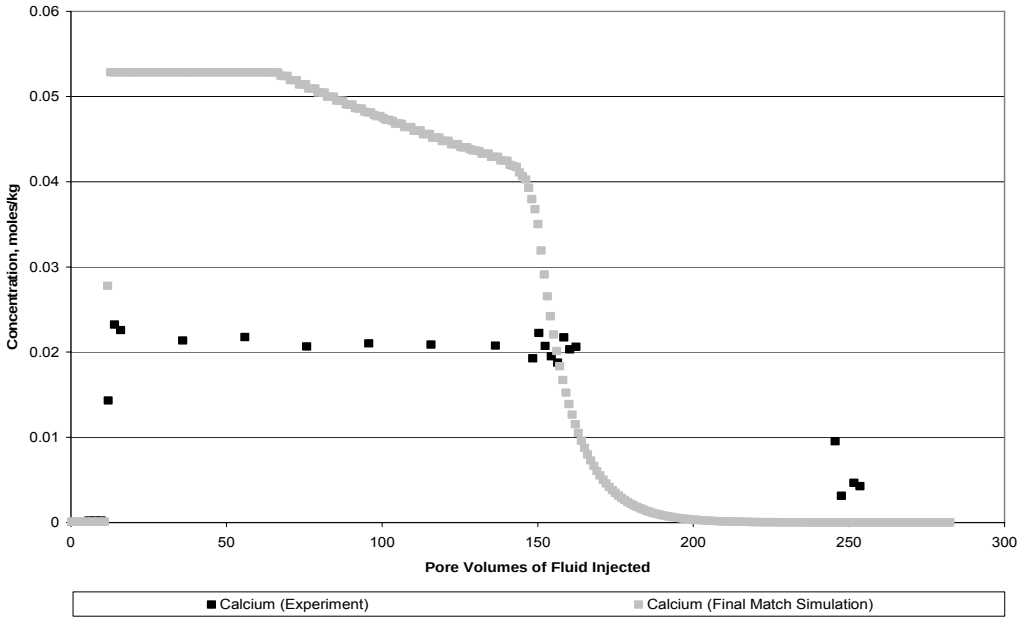

Figure IV-4: Effluent Concentration of Calcium for the Second Core Flood

Figures IV-4, IV-5, IV-6 and IV-7 show the effluent concentrations of calcium, silicon, aluminum and potassium for the second core flood, respectively. Although iron was measured in the experimental effluent, iron was not present in the minerals in the simulation.

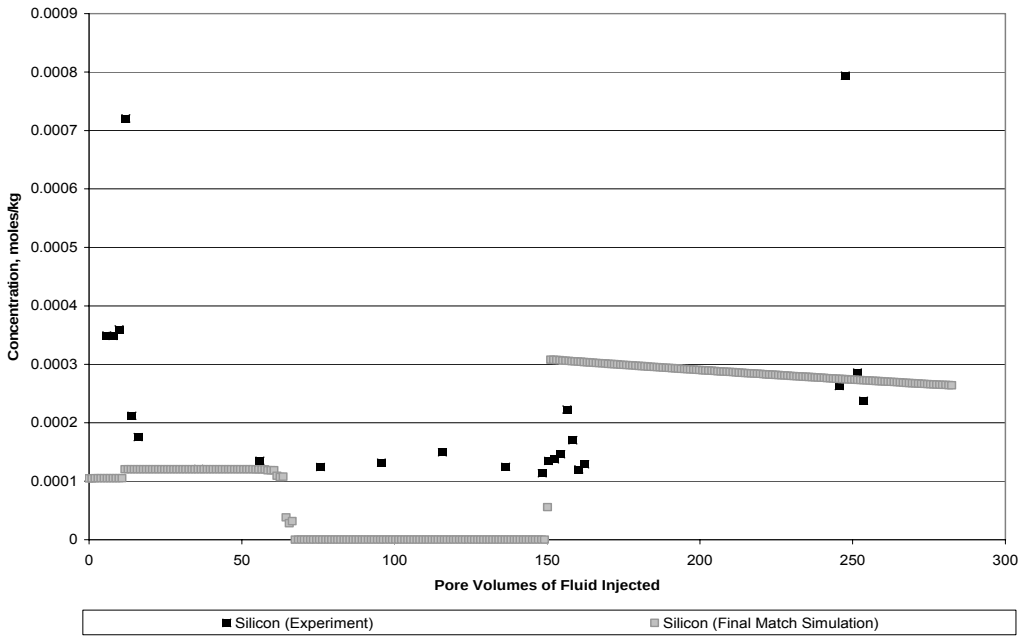

Figure IV-5: Effluent Concentration of Silicon for the Second Core Flood

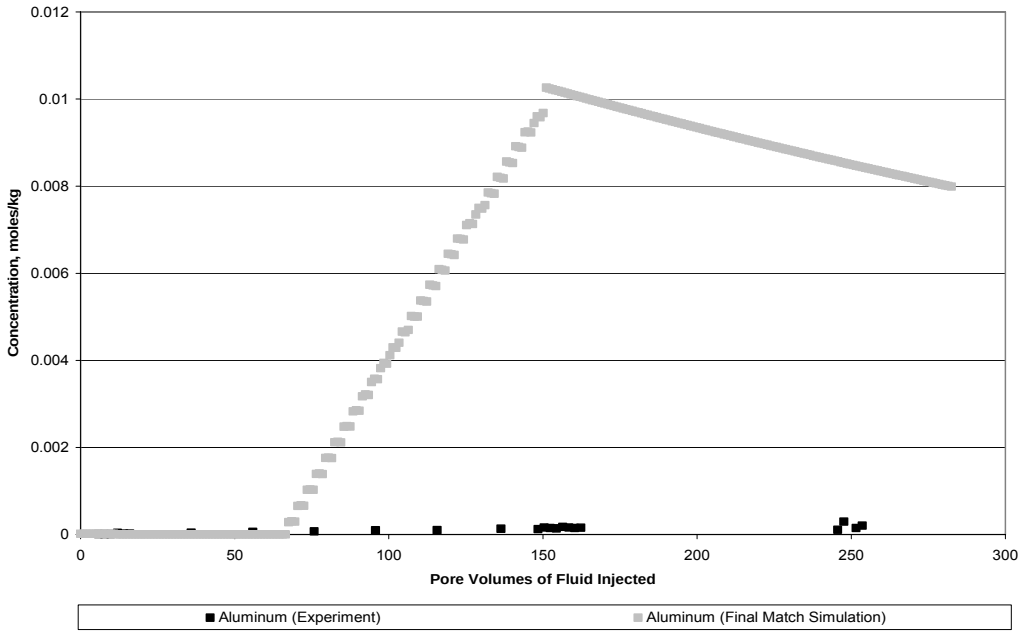

Figure IV-6: Effluent Concentration of Aluminum for the Second Core Flood

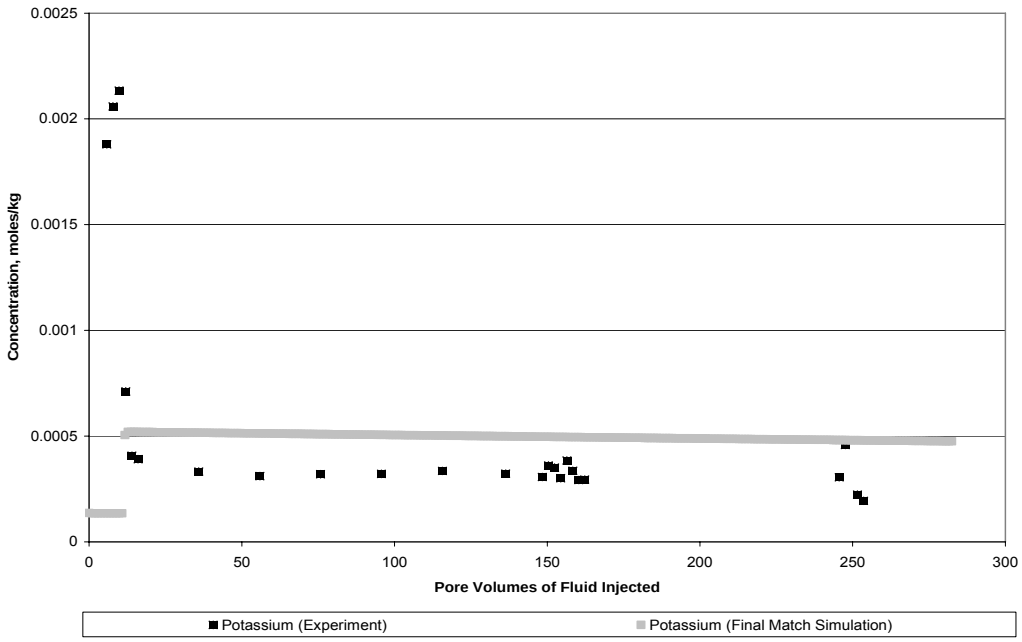

Figure IV-7: Effluent Concentration of Potassium for the Second Core Flood

Discussion of Berea Core Mineralogy and Reaction Coefficients

The history matching procedure used to identify the minerals reacting in the Berea sandstone core and their reaction rates was enlightening with regard to the interaction of the minerals, their concentrations and their reaction rates. The main issues identified are:

- A single mineral model consisting of calcium and a non-reactive mineral can nearly describe the pH trend observed in the second core flood experiment. Such a model requires more calcium than one would expect in a Berea core and would not increase the pH of acid once all the calcium was dissolved.
- While attempting to match the number of pore volumes of acid required to drop the effluent pH from about 5 to 1.5 for the second core flood it became apparent that the mineral concentrations and reaction rates are interrelated. The volume of calcium in the model can be reduced to an extent while matching the number of pore volumes of acid required to cause an effluent pH drop by increasing the reaction rate of the other minerals, or by increasing the calcium reaction rate.
- The presence of calcium and a clay mineral (illite or kaolinite) together causes a significant precipitation-dissolution reaction involving the clay mineral. This precipitation-dissolution reaction can cause a temporary effluent plateau at pH 3 if slower calcium reaction rates are used or if faster clay reaction rates are used. This clay reaction is responsible for the absence of silicon observed in the simulation effluent between the times while 70 to 150 pore volumes were injected as shown in figure 4-5.
- The reaction area equation (equation 3-14) used in GEM slows the dissolution rate of minerals as they deplete. This leaves mineral present behind the dissolution front that dissolves away over time as more acid is injected.
- Future acid injection core flood experiments used to simulation matching exercises should have the effluent concentrations of magnesium and sodium measured, along with any possible measurements to identify complex ions in solution. Such detailed measurements may be useful to identify the reactive clays and ionic species that should be included in geochemical simulations.

Appendix V: Propagating pH-Sensitive Polymer in Petroleum Reservoirs

It is desirable to inject pH-sensitive polymer in reservoirs as a low viscosity acidic fluid for several reasons. It will be shown in chapters six and seven that injecting this polymer as a low viscosity fluid can improve flood conformance. Injecting pH-sensitive polymer as a low pH fluid also increases the injectivity of the polymer. This chapter describes several strategies to place low pH fluids in a reservoir by lowering Damköhler number of the reservoir-acid reactions that occur in situ. The strategies described are increasing the fluid velocity, using an acid pre-flush to consume fast-reacting minerals, using a high acid concentration, and using the pH buffering effect of weak acids. Much of the analysis presented is based on the mineral reaction coefficients found from the history matching process described in the previous chapter. Only the viscosity dependence of pH is covered in this chapter (the effects of ionic strength, shear rate and polymer concentration on polymer viscosity are not addressed here.)

Definition of the Damköhler Number

The Damköhler number, N_{Da}, is a dimensionless number used to compare the reaction rate of acid with a mineral to the acid convection rate. The Damköhler number groups the effect of mineral-acid stoichiometry, kinetics, acid concentration and Darcy velocity into one value. Typically a large N_{Da} (greater than 10) indicates a fast acid reaction compared to the transport rate, whereas a small N_{Da} (less than 1) indicates a relatively slow acid reaction rate. The Damköhler number can be defined in several ways but in this thesis it is defined based on the maximum mineral dissolution rate, r_β, used by GEM-GHG:

$$N_{Da} = \frac{LAr_{H^+}}{1000qa} \qquad [V.1]$$

where L = length of medium (m), A = area perpendicular to flow (m^2), ϕ = initial porosity of porous medium, q = acid flow rate (m3/s), a = H^+ molality (mol/kg), r_{H^+} = reaction rate of H^+ ($mol/m^3 \cdot s$)

The reaction rate of H^+ is directly proportional to the mineral reaction rate by the ratio $\upsilon_{H^+} / \upsilon_{mineral}$. This is the ratio of the number of moles of H+ ions consumed per mole of mineral consumed.

$$r_{H^+} = \frac{\nu_{H^+}}{\upsilon_{mineral}} r_\beta = \frac{\nu_{H^+}}{\upsilon_{mineral}} \left(\mathrm{sgn}\left[1 - \left(\frac{Q_\beta}{K_{eq,\beta}} \right) \right] \right) \hat{A}_\beta S_w \left(\mathrm{k}_{0,\beta} + \sum_{i=1}^{n_{aq}} k_{i,\beta} a_i^{\omega,\beta i} \right) \left| 1 - \left(\frac{Q_\beta}{K_{eq,\beta}} \right)^{\xi_\beta} \right|^{\varsigma_\beta} \qquad [V.2]$$

Sample calculations for the Damköhler number and a mineral reaction rate are given in Appendix 1. The Damköhler number for a radial system varies with distance from the well since the flow area changes as a function of distance from the well bore.

Propagating Acidic Fluids in Reactive Porous Media

Experiments clearly show that hydrochloric acid reacts with Berea sandstone to increase the pH of the acid while metal cations were liberated from the sandstone. Acid-matrix chemical reactions cause a low pH front to travel slower than the injected fluid front (salinity front).

Injection of acidic pH-sensitive polymer into a reservoir may experience a large viscosity increase in situ unless the Damköhler number of the matrix-acid reaction is reduced to a low value to allow the polymer to travel at its minimum viscosity. The Damköhler number can be reduced by increasing the acid velocity or proton concentration or by decreasing the acid or polymer transport distance or the net hydrogen consumption rate (r_{H^+}). The net hydrogen consumption rate can be effectively reduced by using an acid preflush to consume the fast reacting mineral(s), like carbonate minerals in the case of Berea sandstone, which leaves the slow reacting minerals behind. The net hydrogen consumption rate can be reduced while the geochemical reaction rates stay constant by injecting a high concentration of a weak acid like acetic acid or citric acid that releases protons as they are consumed by the reservoir minerals. Numerical simulation or detailed calculations should be favored over Damkholer number calculations to assess the in situ pH of a polymer treatment. This is because a low Damkohler number can be calculated for a reaction even if the injected acid has a pH close to or above that required to swell pH-sensitive polymer.

Simulations

The simulation results presented in this chapter are based on the "final match" mineralogy, aqueous species and reaction coefficients determined in chapter four. A linear one dimensional grid consisting of 200 cells in the x-direction was used. Each cell has a porosity of 0.177 and dimensions of 0.5 m, 2.377 m, and 2.377 m in the x, y, and z directions, respectively. The total pore volume of the model is 100 m^3 and there is a constant rate acid injector in cell 1 and a constant pressure producer in cell 200. All cases start with a brine filled reservoir with a pH of 10.23.

Effect of In Situ Acid Velocity

Changing the acid flow velocity by modifying the injection rate or cross-sectional flow area is one way of changing the Damkohler number of a reaction. The figure below demonstrates the effect of varying the flow velocity of pH 1 hydrochloric acid flowing through a linear grid. The dimensionless distance shown is the distance from the injection well divided by the reservoir length (100 m.) The dimensionless concentration of non-reactive chloride is shown to demonstrate the mixing effect between the acid and reservoir brine near the end of the reservoir in the 0.3 m/d velocity run.

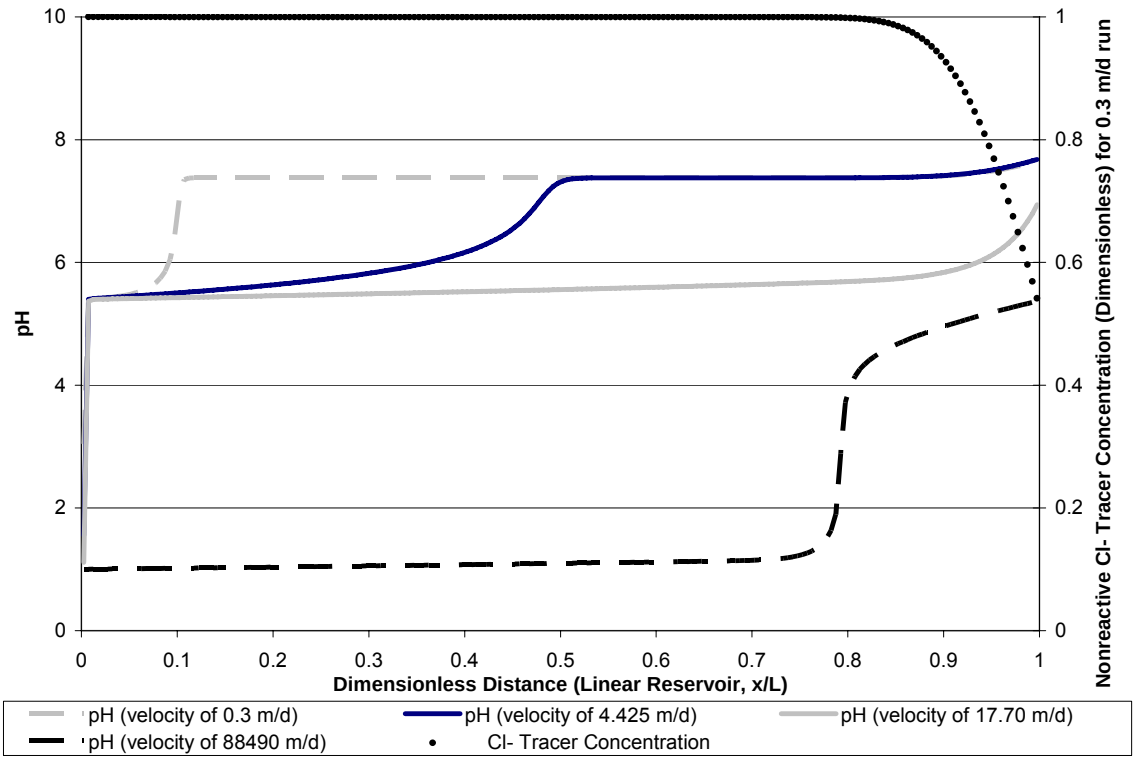

Figure V-1: In-Situ pH versus Dimensionless Distance After Injecting One Pore Volume of Hydrochloric Acid at Various Velocities

Effect of Acid Concentration

The Damkohler number of an acid-matrix reaction can be decreased by increasing the concentration of the acid injected. The following figure shows the in situ pH profile as a function of dimensionless distance for various concentrations of hydrochloric acid injected at 25 m^3/d. The injected acids had a concentration of 1 molal, 0.1 molal and 0.01 molal giving acid pHs of 0, 1, and 2, respectively. Dimensionless Cl^- tracer concentration is shown for the pH 2 acid injection case.

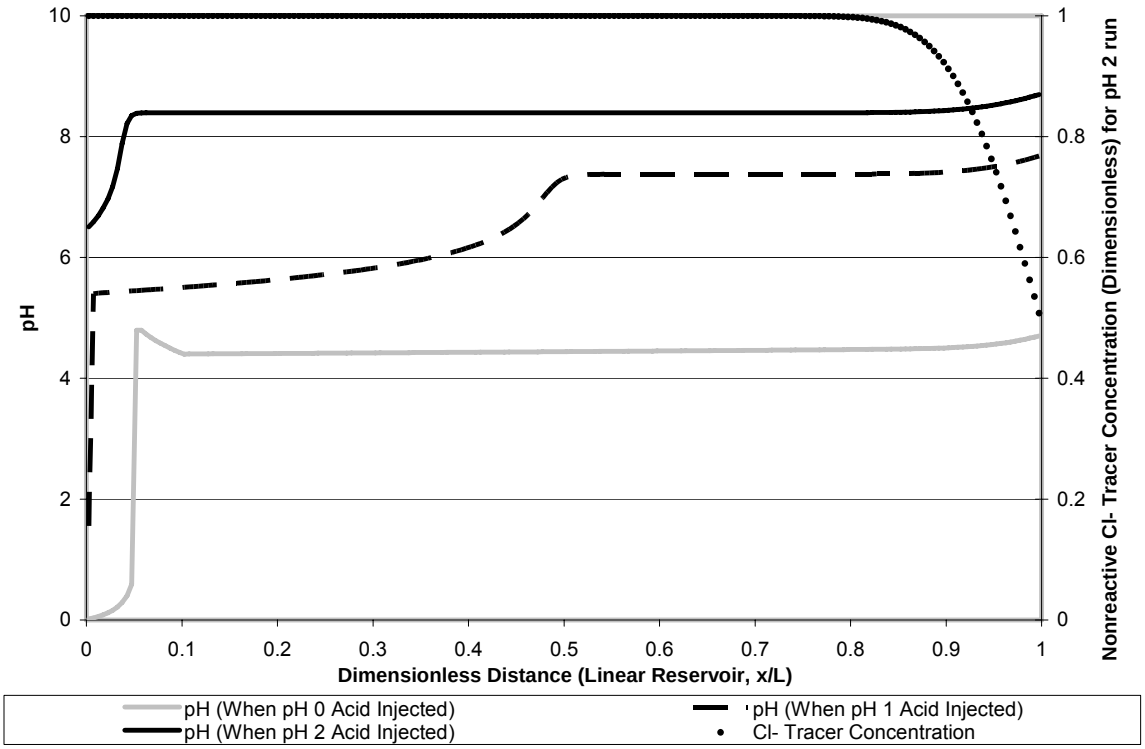

Figure V-2: In-Situ pH versus Dimensionless Distance After Injecting One Pore Volume of Strong Acid With Various Concentrations

The unusual local pH increase at the distances from 0.05 to 0.10 is caused by mineral precipitation of the kaolinite from solution. This can be confirmed by figure 5-3 that shows the mineral concentrations as a fraction of their initial values. From the equation in table 4-3 the precipitation reaction for kaolinite is $2\ Al_3{}^{+}{}_{(aq)} + 2\ H_4SiO_{4(aq)} + H_2O \rightarrow Al_2Si_2O_5(OH)_{4(s)} + 6\ H^{+}{}_{(aq)}$. Figure 5-4 shows the falling $Al_3{}^{+}{}_{(aq)}$ and $H_4SiO_{4(aq)}$ concentration associated with the precipitation reaction.

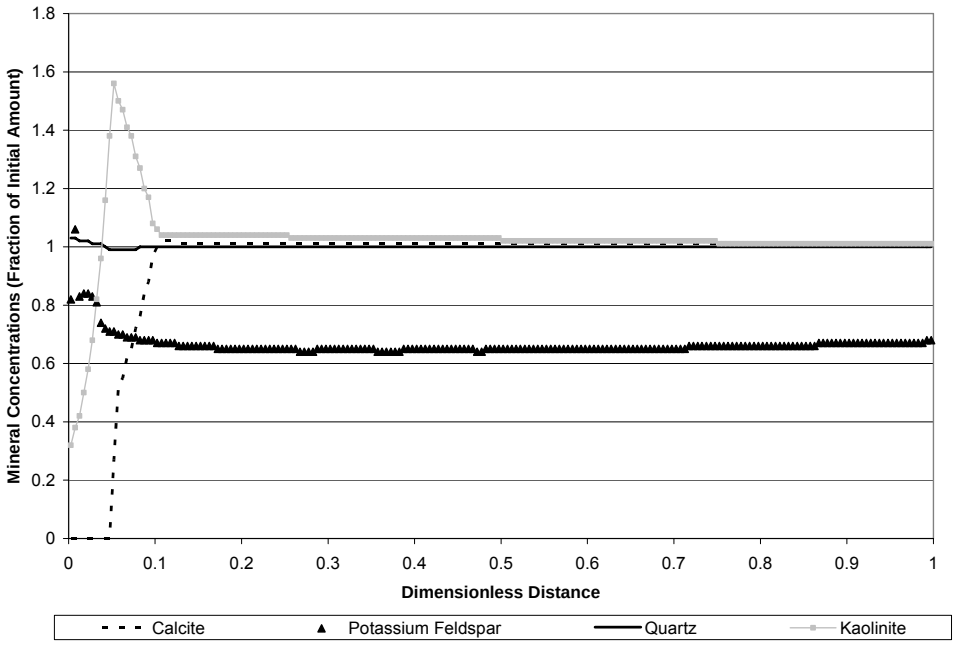

Figure V-3: Dimensionless Mineral Concentrations versus Dimensionless Distance After Injecting One Pore Volume of Hydrochloric Acid

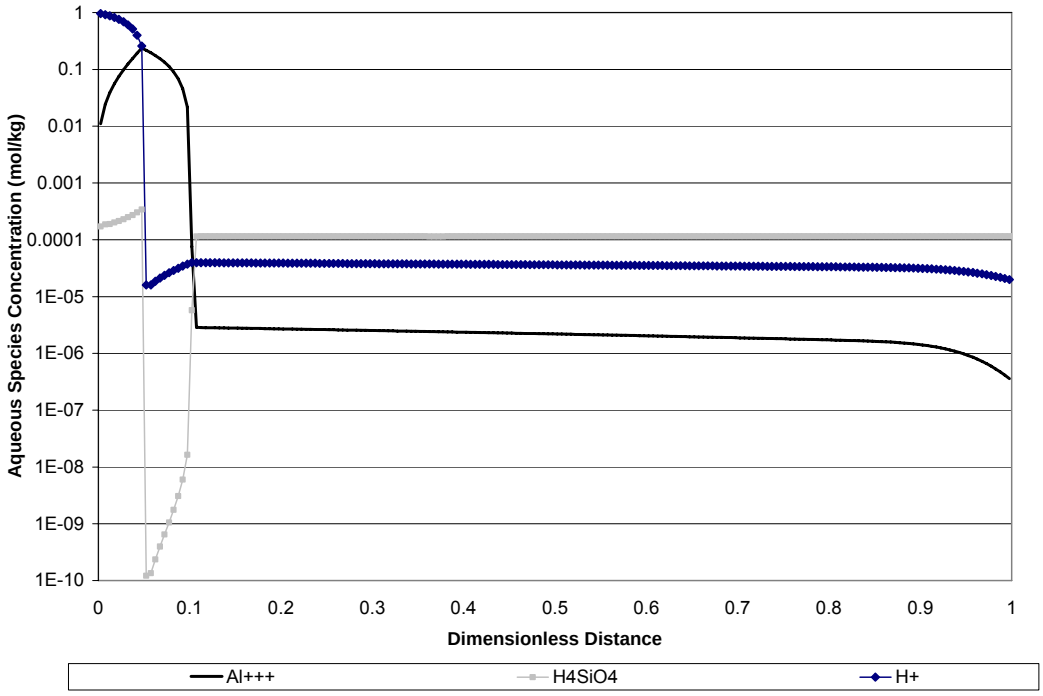

Figure V-4: Al^{+++}, H_4SiO_4 and H^+ Species Concentrations versus Dimensionless Distance After Injecting One Pore Volume of Hydrochloric (pH =0) Acid

Effect of Acid Preflush

A low pH fluid front can be propagated by injecting a large volume of acid to consume the fast reacting mineral(s) in the reservoir. pH fronts will travel through the reservoir as injection proceeds. A simulation was performed with pH 1 hydrochloric acid being injected continuously into a linear reservoir.

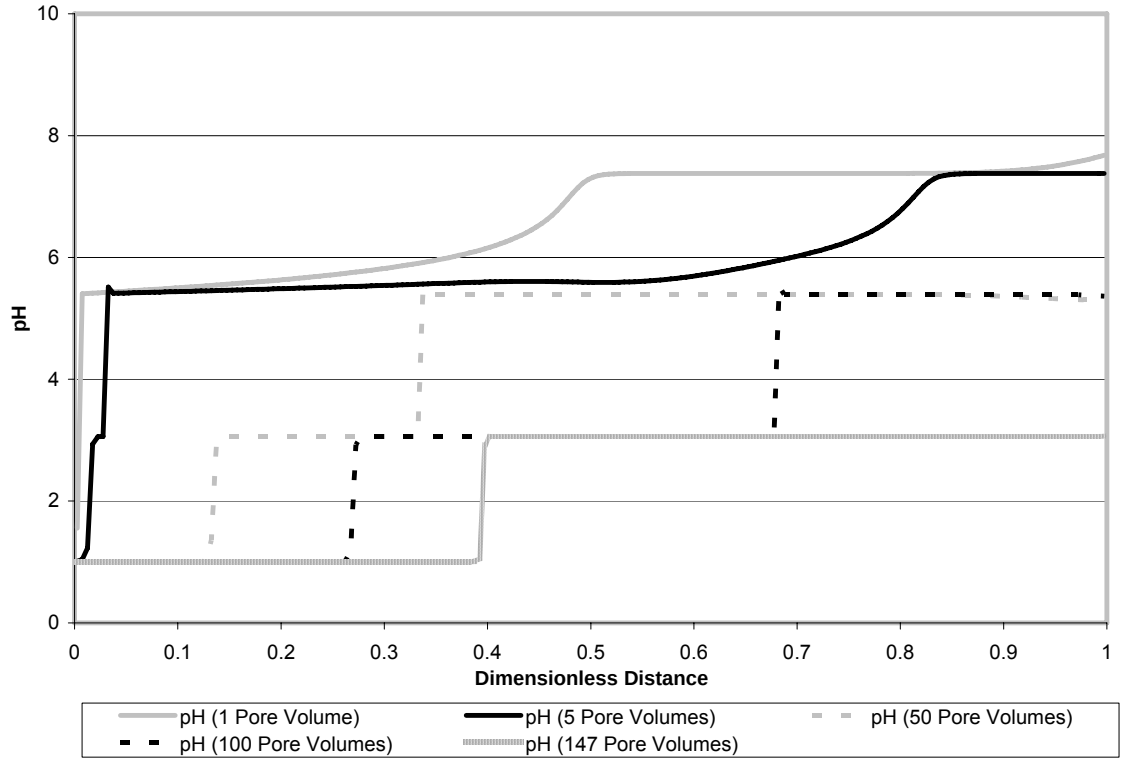

Comparison of Strong Acid to Weak Acids

Strong acids ionize almost completely in water whereas weak acids only partially dissociate. Simulations were performed to examine the pH profile resulting from injecting a strong acid (hydrochloric acid) and two different weak acids (acetic acid and citric acid). The dissociation reactions and equilibrium constants below are employed in the simulations (at 25ºC). Only the reactions required for a simulation were included in it.

Hydrochloric Acid

$HCl_{(aq)} \rightarrow H^+_{(aq)} + Cl^-_{(aq)}$ Assumed fully dissociated [V.3]

$H^+_{(aq)}$ and $Cl^-_{(aq)}$ were injected directly into reservoir in the aqueous phase

Acetic Acid

$CH_3COOH_{(aq)} \rightarrow H^+_{(aq)} + CH_3COO^-_{(aq)}$ $K_{eq} = 10^{-4.756}$ [V.4]

Citric Acid

$C_6H_8O_{7(aq)} \rightarrow H^+_{(aq)} + C_6H_7O_7^-{}_{(aq)}$ $K_{eq} = 10^{-3.128}$ [V.5]

$C_6H_7O_7^-{}_{(aq)} \rightarrow H^+_{(aq)} + C_6H_6O_7^{2-}{}_{(aq)}$ $K_{eq} = 10^{-4.761}$ [V.6]

$$C_6H_6O_7^{2-}{}_{(aq)} \rightarrow H^+{}_{(aq)} + C_6H_5O_7^{3-}{}_{(aq)} \qquad K_{eq} = 10^{-6.396} \qquad [V.7]$$

Figure V-5 shows the in situ pH profile for 1.0 molal concentrations of hydrochloric acid, acetic acid and citric acid after one pore volume of acid was injected at a rate of 25 m^3/d. At these concentrations the injected acids had pHs of 0, 2.4 and 1.6, respectively.

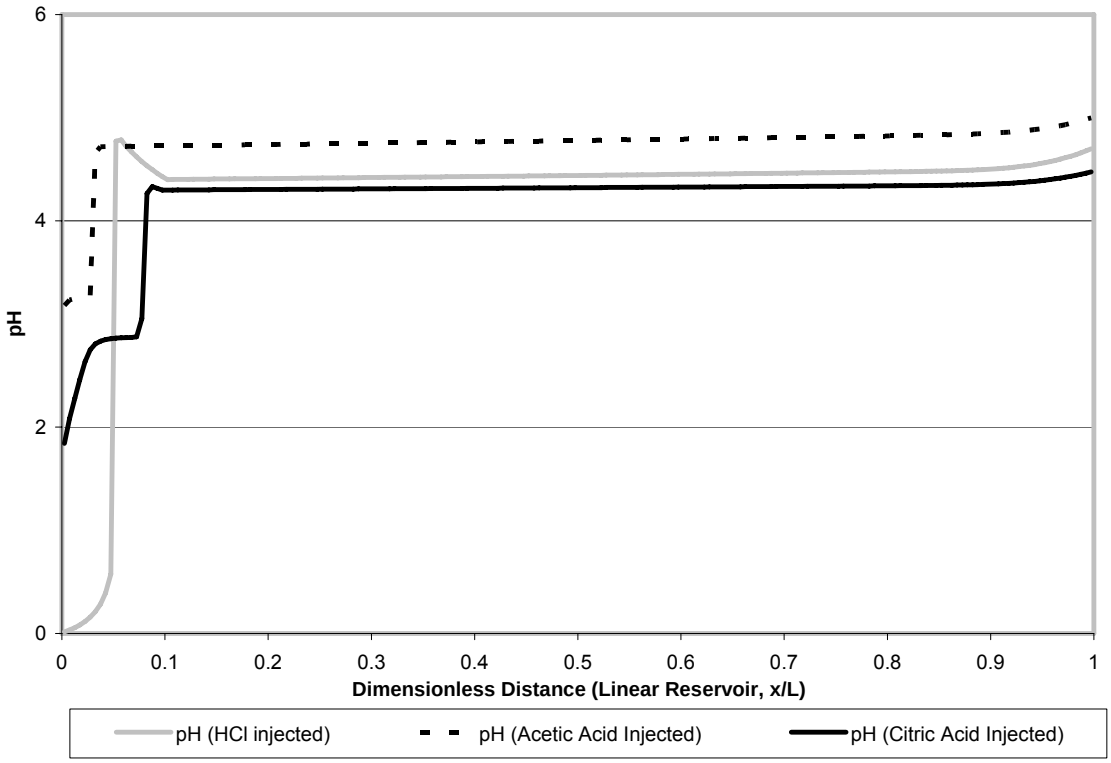

Figure V-5: In Situ pH versus Dimensionless Distance After Injecting One Pore Volume of 1.0 Molal Concentration Acid for Various Acids

Stronger acids are better suited for maintaining a low pH in the reservoir compared to weak acids with similar concentrations. Figure V-6 shows the in situ pH profile after injecting pH 2 hydrochloric acid, acetic acid and citric acid into Berea (at a rate of 25 m^3/d) at concentrations of 0.010 molal, 5.71 molal and 0.144 molal, respectively. The weaker acids maintain a low pH for a longer distance but require much higher concentrations than the strong acid.

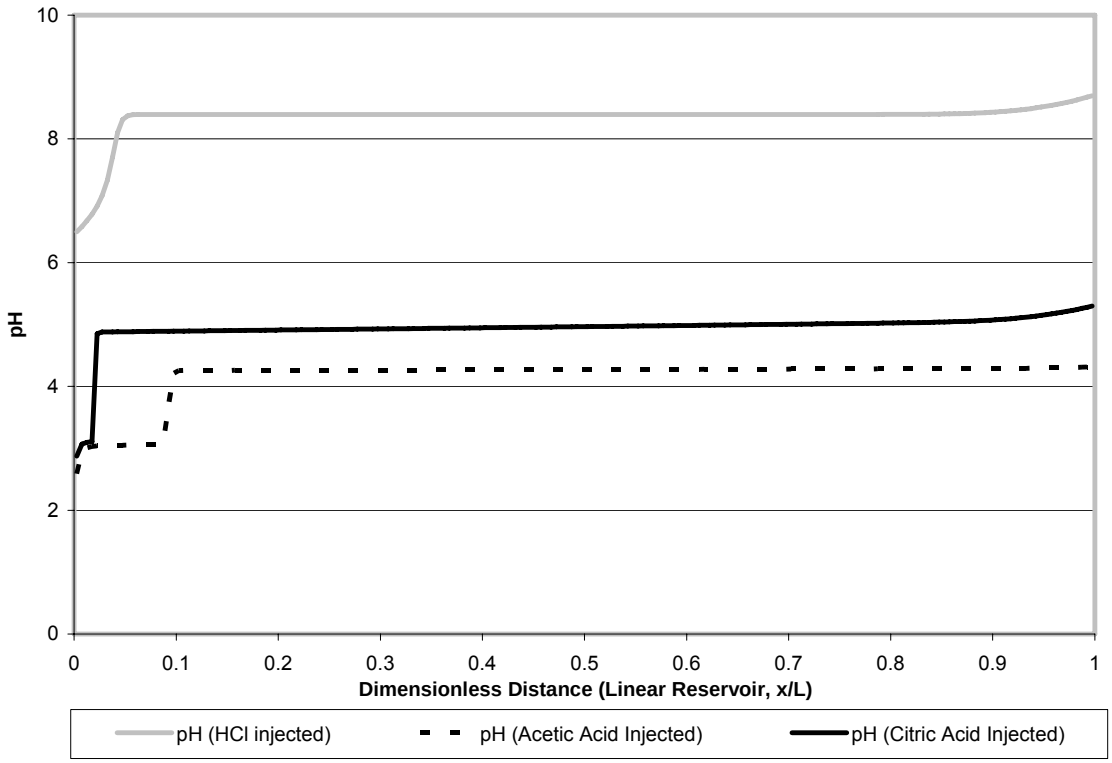

Figure V-6: In Situ pH versus Dimensionless Distance After Injecting One Pore Volume of pH 2 Acid Solutions of Hydrochloric, Acetic and Citric Acid

The injector in the pH 2 acid injection runs was shut in after one pore volume of acid was injected, and the simulations were continued to monitor the pH in the reservoir as a function of time after the shut in time. Figure V-7 shows the pH in grid cell 100 (distance 0.4975) as a function of time. It took 0, 60 and 76 days for the hydrochloric, acetic and citric acid to approach equilibrium with the Berea reservoir, with final brine pHs of 7.38, 4.46 and 5.56, respectively.

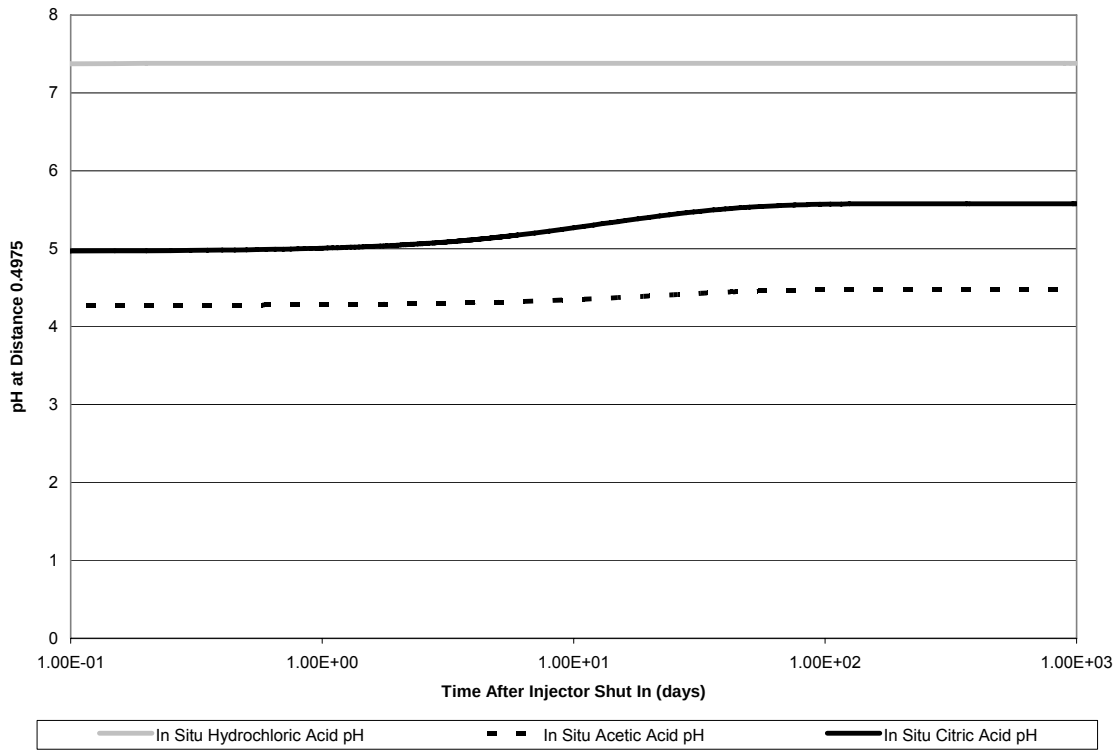

Figure V-7: pH versus time after injection of pH 2 Acid Solutions of Hydrochloric, Acetic and Citric Acid was stopped

Comparison of Linear and Radial Flow Geometry

A simulation was run with a radial grid with a pore volume of 100 m^3 to compare the in situ pH profile with the linear grid after injecting one pore volume of pH 1 strong acid at a rate of 25 m^3/d. The radial grid is one dimensional with a porosity of 0.177, a height of 2.377 m, an inner radius of 0.1 m and an outer radius of 8.699 m, with 200 radial grid cells with lengths increasing logarithmically away from the inner radius. A dimensionless area scale was devised to compare the pH profiles on an equivalent basis. The dimensionless area is the cumulative area from the injector to the center of a given grid cell, divided by the total grid area.

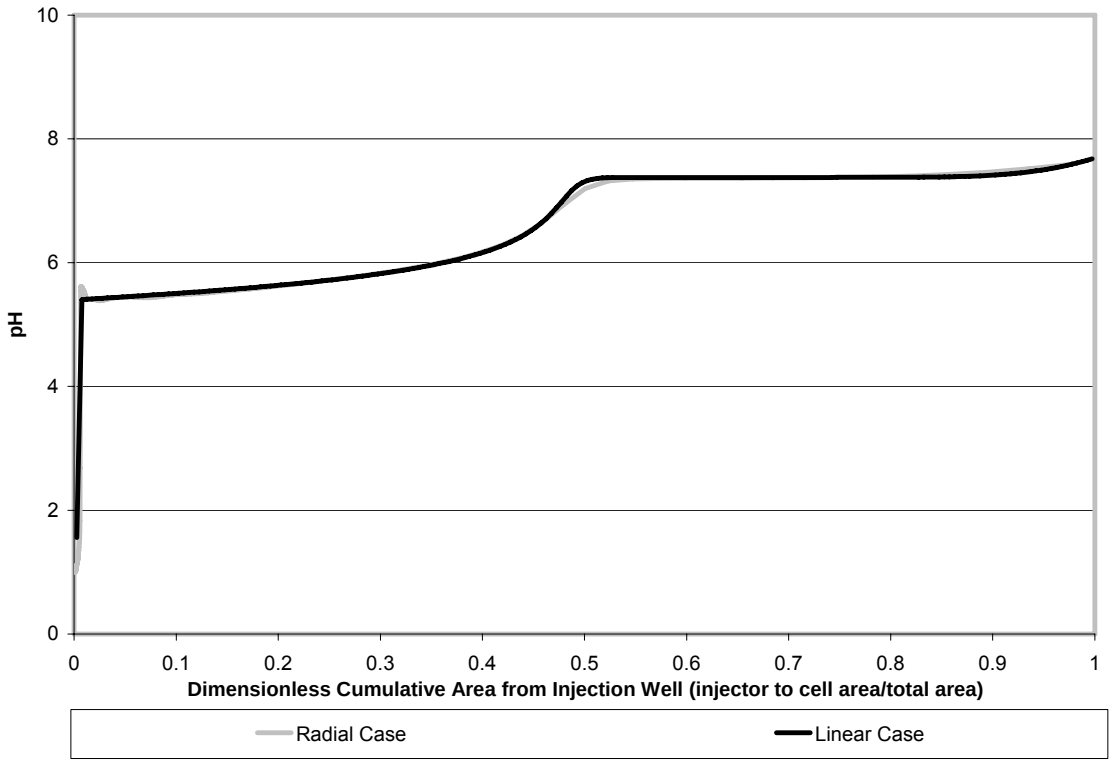

Figure V-8: pH versus Dimensionless Area After Injecting One Pore Volume of pH 1 Hydrochloric Acid

The linear and radial grids have nearly the same pH distribution when compared in terms of area from the injector at the given injection rate. This similarity may be useful for translating pH profiles from linear cases to radial cases though no work has been done to confirm this relationship holds at other operating conditions.

Appendix VI
In-Depth Conformance Control Using pH-Sensitive Polymer

Most oil reservoirs depend on a fluid displacement mechanism to maximize oil recovery. Conformance control is usually identified as a means of improving the recovery efficiency of such flooding operations. This chapter covers in-depth conformance control using conventional polymers (i.e. HPAM, xanthan, etc.) and pH sensitive polymers for linear reservoirs with multiple layers. The fractional flow allocation into each of a reservoir's horizontal layers is described as a means to evaluate the effectiveness of various in-depth conformance control strategies. The problems associated with waterflooding reservoirs comprised of multiple layers with varying permeabilities are presented. The benefits of injecting a high viscosity fluid as a flooding agent, usually a polymer, are quantified for a set of simplified conditions. The benefits of using pH-sensitive polymer are discussed along with the conditions found to make the polymer treatment most effective. All cases in this chapter focus only on the ability of the conformance control methods to recover oil by diverting injected fluid from higher permeability layers into lower permeability layers. Polymer adsorption and relative permeability are neglected, and cross flow is only treated briefly.

Fractional Flow Allocation (FFA)

Most of the discussion in this chapter deals with simplified linear reservoirs comprised of two or more horizontal layers arranged in a stack. An injector well is assumed to be completed into all the layers at one end of the reservoir, and a producing well is assumed to be completed into all the layers at the other end of the reservoir. Each layer is assumed to have homogenous permeability (k) and porosity (Φ) throughout, although each layer may have a different permeability, porosity and height (h). When the layers do not allow flow in a vertical direction there is said to be "no cross-flow" between the layers. Likewise, the layers have "cross-flow" when fluid can flow vertically between them.

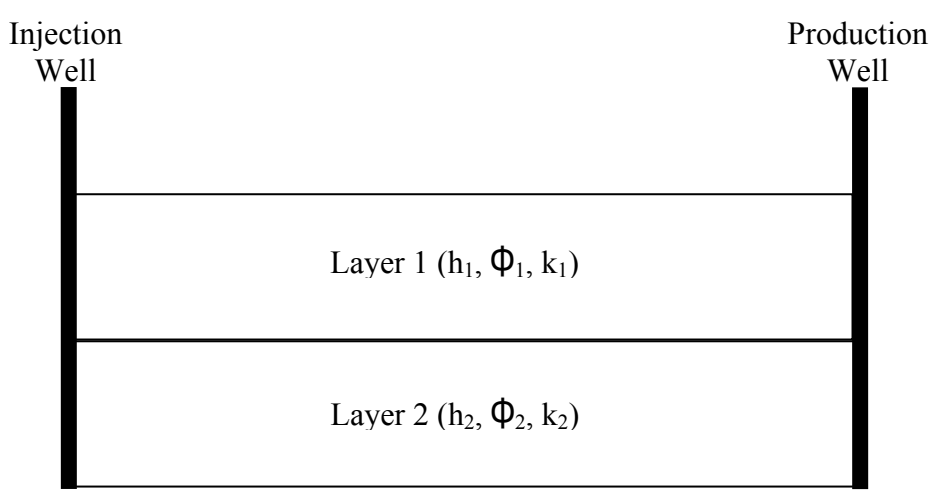

Figure VI-1 Simplified Linear Reservoir with Multiple Horizontal Layers

When fluid is injected into the injection well, the fluid will flow into the different layers at different rates depending on the reservoir layer properties and the viscosity of the injected fluid and the fluid in each layer. Since the fluid rate into each layer (q_i) may change over time it is useful to calculate the fractional flow allocation, f, into each layer at any given time. This is fraction of the total injected fluid rate (Q) that is injected into any given layer in an n-layer reservoir:

$$f_i = \frac{q_i}{Q} = \frac{q_i}{\sum_{j=1}^{n} q_j} \qquad \text{[VI.1]}$$

Ideal conformance of a flooding operation has the injected fluid traveling at an equal velocity in each layer. In such a case all the mobile oil will be recovered with no early breakthrough of the injected fluid assuming piston like fluid displacement. The fractional flow allocation for each layer corresponding to ideal conformance is related to the height of each layer:

$$f_{i,ideal} = \frac{q_{i,ideal}}{\sum_{j=1}^{n} q_{j,ideal}} = \frac{(v_{ideal})(width)}{(v_{ideal})(width)} \frac{h_{i,ideal}}{\sum_{j=1}^{n} h_j} = \frac{h_{i,ideal}}{\sum_{j=1}^{n} h_j} \qquad \text{[VI.2]}$$

This applies to multi-layered reservoirs of linear and radial geometry with no cross-flow.

Waterflooding Linear Reservoirs

Water is a commonly used fluid for flooding oil reservoirs due to its availability, low cost, and ease of use. The viscosity of water is often close to that of light oils (about 1 cp), although many oils have a viscosity several orders of magnitude greater than water. If it is assumed that water and oil have the same viscosity then the fractional flow into each layer can be calculated using Darcy's law to get the following result:

$$f_i = \frac{k_i h_i}{\sum_{j=1}^{n} k_j h_j} \qquad \text{[VI.3]}$$

This result is valid for all times for multi-layered reservoirs with linear and radial geometry and no cross-flow. If the density difference between oil and water is neglected along with relative permeability effects then this result is true for the cross-flow case as well. It can be observed that layers with a very high permeability will take most of the injected fluid at the expense of the low permeability layers. It is in these cases that the higher permeability layers are called thief zones and where a conformance control method is desired to divert fluid into the lower permeability layers.

High Viscosity Fluid Injection as a Conformance Control Method (No Cross-flow Case)

The use of polymers like HPAM and Xanthan gum to increase the viscosity of the injected fluid does help divert flow from high permeability zones to low permeability zones which increases conformance of a polymer flood. Some published polymer flooding field tests have been conducted at the Loudon field (Huh *et al.*, 1990), Chateaurenard field (Takagi et al., 1992) and Hankensbuettel field (Baviere, 1991). The effect of injecting a high viscosity polymer (relative to the in situ oil viscosity) on the fractional flow allocation into each layer

in the absence of cross-flow can be calculated for a multi-layer linear reservoir by assuming piston-like displacement of the oil by the polymer and by employing Darcy's law. These calculations and the associated assumptions are given in Appendix 2 and yield the following result:

$$f_i = \frac{q_i}{\sum_{i=1}^{n} q_i} = \frac{\left(\dfrac{k_i h_i}{\sqrt{(\mu_1 L)^2 + 2(\mu_2 - \mu_1)\dfrac{k_i}{\phi_i}(\int \Delta P dt)}} \right)}{\left(\sum_{i=1}^{n} \dfrac{k_i h_i}{\sqrt{(\mu_1 L)^2 + 2(\mu_2 - \mu_1)\dfrac{k_i}{\phi_i}(\int \Delta P dt)}} \right)} \qquad \text{[VI.4]}$$

Logic suggests that maximum conformance control can be achieved by injecting a fluid with infinite viscosity . The fractional flow allocation into each layer of a linear reservoir with an infinitely viscous Newtonian fluid can be calculated by taking the limit as the injected viscosity approaches infinity. Such a calculation has been performed and the results are that the fractional flow allocation approaches the following limit for layer i:

$$f_i = \frac{h_i \sqrt{\phi_i k_i}}{\sum_{j=1}^{n} h_j \sqrt{\phi_j k_j}} \qquad \text{[VI.5]}$$

A similar result has been found by Sorbie and Mackay (2005) except that their result did not include the layer porosities. Both equations [VI.4] and [VI.5] are only valid until the injected fluid front in the any of the layers arrives at the producing well.

Simulations were performed for a linear reservoir with the following parameters to demonstrate the FFA of a waterflood and a conventional polymer. The same reservoir is used to demonstrate the effect of using pH sensitive polymer.

Table VI-1 Linear Reservoir Simulation Grid Properties (No Crossflow)

Reservoir Property	Layer 1 (top)	Layer 2 (bottom)
Porosity	0.177	0.177
Height	10 m (k-dir, 1 cell)	1 m (k-dir, 1 cell)
Length	100 m (x-dir, 100 cells)	100 m (x-dir, 100 cells)
Width	51.361 m (y-dir, 1 cell)	51.361 m (y-dir, 1 cell)
X-dir Permeability	10 md	1000 md
Y-dir Permeability	10 md	1000 md

Z-dir Permeability	0 md	0 md
Initial Fluid Properties	$S_w = 1$, $\mu_w = 1$ cp	$S_w = 1$, $\mu_w = 1$ cp
Grid Pore Volume	10000 m^3 total	

The reservoir initially contained 1 cp water (to represent a light oil with no relative permeability effects) with a pH of 10.23 and the "final match" mineral reaction parameters.

The following fractional flow allocation profiles were generated as a function of dimensionless time (number of pore volumes injected) for the injection of 1 cp water and for the injection of a 100 cp polymer. The analytical solution came from equation [VI.4], with an adjustment made for post-breakthrough times. The FFA at times before 0.1 pore volumes injected is approaches the value of 0.5 calculated for each layer from equation [VI.5].

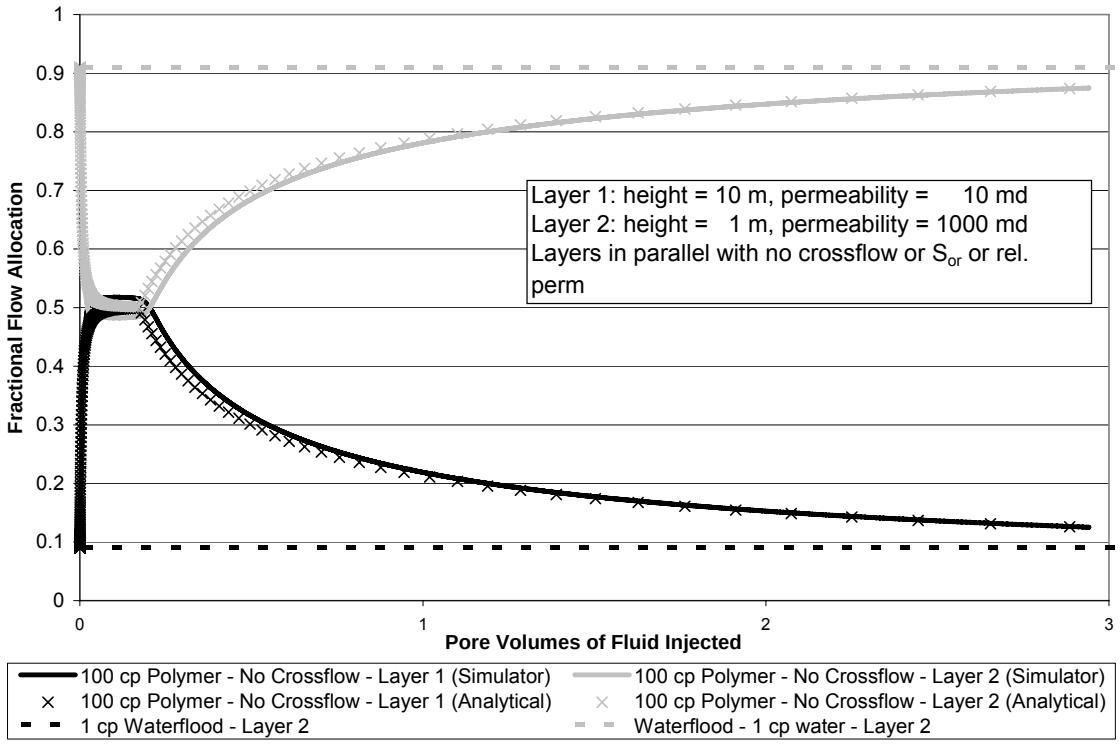

Figure VI-1 Fractional Flow Allocation into Two Layer Reservoir for Waterflood and 100 cp Polymer Flood

Appendix VII
Injection Well Vertical Conformance with Use of a pH-Sensitive Polymer

VII.1. Introduction

This Appendix has two objectives: the first is the preliminary evaluation of the effectiveness of the pH-sensitive polymer injection as a way of improving vertical conformance at injection wells, in particular, compared to the injection of a conventional polymer solution. This aspect of study will be, therefore, an extension of the earlier study by Reznik *et al*. (1984) and by Sorbie and Mackay (2005). The second objective is to outline an initial, simplified version of a computer program that helps optimize the vertical conformance control application of the *p*H-sensitive polymer at an injection well. In applying the *p*H-sensitive polymer technique, we need to understand how the polymer injected at the well is allocated into each reservoir layer, and how the allocation changes with time.

The following model assumptions are made:

- Only brine phase is present, which contains polymer, H^+, mineral anions, and a tracer.
- Solid phase is assumed to include only two mineral components (slowing and fast reacting), which dissolve into brine as anions and react with H^+. The number of mineral components could be of course be increased, with only minor modification of the program.
- The injection well feeds into multiple reservoir layers, which are assumed to be non-communicating.

VII.2. Injection Allocation

The allocation of injected fluids into each reservoir layer will be first considered. Under the steady-state condition, the material balance for the injected water in the *i*-th layer is

$$u_i = \frac{Q_i}{2\pi h_i r} = \left(\frac{Q_t}{2\pi h_i}\right)\frac{f_i}{r} \qquad \text{[VII.1]}$$

where u_i is Darcy velocity, Q_i is injection rate, and h_i is thickness, all for the *i*-th layer; and $f_i \equiv Q_i/Q_t$ is the injection allocation into the *i*-th layer, and Q_t is the total injection rate. By integrating the Darcy's equation

$$u_i = -\frac{k_i}{\mu_i}\frac{\partial p}{\partial r} \qquad \text{[VII.2]}$$

we obtain

$$p_w - p_o \equiv \Delta p = \left(\frac{Q_t}{2\pi k_i h_i}\right) f_i \int_{r_w}^{r_o} \mu_i \frac{dr}{r} \qquad \text{[VII.3]}$$

where k_i is permeability and μ_i is viscosity for the *i*-th layer; and p_w and p_o are pressure at the wellbore radius (r_w) and the outer boundary radius (r_o), respectively.

When only acid is injected, the water viscosity is constant, $\mu_i = \mu_{wo}$, so that

$$\Delta p = \frac{\mu_{wo} Q_t f_i}{2\pi k_i h_i} \ell n\left(\frac{r_o}{r_w}\right) \qquad \text{[VII.4]}$$

If we define the average permeability for the reservoir as

$$k_a \equiv \frac{1}{H}\sum_{i=1}^{N} k_i h_i \qquad \text{[VII.5]}$$

where $H \equiv \sum_{i=1}^{N} h_i$ is the total thickness, we obtain

$$f_i = \frac{2\pi k_i h_i \Delta p}{\mu_{wo} Q_t \ell n\left(\frac{r_o}{r_w}\right)} = \frac{k_i h_i}{k_a H} \equiv f_{ni} \qquad \text{[VII.6]}$$

That is, the injection allocation is according to the fraction of (permeability x thickness), f_{ni}. Without polymer injection, the injection allocation for each layer follows Eq.[VII.6], and does not change with time. The Darcy velocity in the above equation can be expressed, from Eqs.[VII.1] and [VII.6],

$$u_i = \left(\frac{Q_t f_{ni}}{2\pi h_i}\right)\frac{1}{r} \qquad \text{[VII.7]}$$

When polymer is injected, the polymer solution viscosity, μ_i, is not constant but now is a function of Darcy velocity, and of concentrations of polymer and hydrogen ion. The Darcy velocity now becomes, from Eqs.[VII.1], [VII.3] and [VII.6],

$$u_i = \frac{\left(\frac{Q_t f_{ni}}{2\pi h_i}\right) B_i \ell n\left(\frac{r_o}{r_w}\right)}{r\int_{r_w}^{r_o}\left(\frac{\mu_i}{\mu_{wo}}\right)\frac{dr}{r}} \qquad \text{[VII.8]}$$

The injection allocation can be calculated as

$$f_i = \frac{f_{ni} \ell n\left(\frac{r_o}{r_w}\right)}{\int_{r_w}^{r_o}\left(\frac{\mu_i}{\mu_{wo}}\right)\frac{dr}{r}} \qquad \text{[VII.9]}$$

When the mixture of the polymer and acid is injected, the injection allocation into each layer therefore varies with time, because the polymer viscosity in the reservoir changes with time and location.

VII.3. Transport of Polymer and Acid in Porous Media

The transport equation for hydrogen ion with concentration of C_{hi} (for the i-layer) is

$$\phi \frac{\partial C_{hi}}{\partial t} + u_i \frac{\partial C_{hi}}{\partial r} = \frac{D_h}{r} \frac{\partial}{\partial r}\left(r \frac{\partial C_{hi}}{\partial r} \right) + \sum_{j=1}^{N} r_j S C_{hi} (C_{je} - C_{ji}) \qquad \text{[VII.10]}$$

where t is time; r is radial distance; ϕ is porosity; D_h is the dispersion coefficient; and r_j is the reaction constant for the j-component mineral of the rock; S is specific surface area of rock available for reaction; C_{je} is the j-component equilibrium concentration observable on the rock surface; C_{ji} is its bulk concentration in pore space. In the present study, we limit the number of mineral components that react with acid to only two: $j = 1$, slow reacting; and $j = 2$, fast reacting.

The j-component mineral transport equation is

$$\phi \frac{\partial C_{ji}}{\partial t} = -r_j S C_{hi} (C_{je} - C_{ji}) \qquad \text{[VII.11]}$$

The total amount of the j-component mineral per unit volume of reservoir rock, q_{ji}, is assumed to be known:

$$q_{ji} = -\phi \int_0^t \frac{\partial C_{ji}}{\partial t} dt = -\phi \left[C_{je} - C_{ji}(t_c) \right] = -\phi (C_{je} - C_{jic}) \qquad \text{[VII.12]}$$

where C_{jic} is the concentration when all of q_{ji} is consumed by reaction with acid (at $t = t_c$). For $t > t_c$, there will be no more reaction.

As a reference to track how the acid front and polymer front propagate, it is convenient to include a non-reacting tracer. The transport equation for tracer with concentration of C_{ti} is

$$\phi \frac{\partial C_{ti}}{\partial t} + u_i \frac{\partial C_{ti}}{\partial r} = \frac{D_t}{r} \frac{\partial}{\partial r}\left(r \frac{\partial C_{ti}}{\partial r} \right) \qquad \text{[VII.13]}$$

where D_t is the dispersion coefficient.

The transport equation for polymer with concentration in water of C_{pi} is

$$\phi \frac{\partial C_{pi}}{\partial t} + \frac{\partial A_i}{\partial t} + \frac{\partial \sigma_i}{\partial t} + u_i \frac{\partial C_{pi}}{\partial r} = \frac{D_p}{r} \frac{\partial}{\partial r}\left(r \frac{\partial C_{pi}}{\partial r} \right) \qquad \text{[VII.14]}$$

where A_i is the adsorption of polymer on pore wall; and σ_i is the trapping, or deep-bed filtration, of polymer. The adsorption is represented with a Langmuir isotherm:

$$A_i = \frac{a_1 C_{pi}}{1 + a_2 C_{pi}} \qquad \text{[VII.15]}$$

For the present simplified derivation, we assume $\frac{\partial \sigma_i}{\partial t} \approx 0$.

When an acid such as HCl is injected into a carbonate reservoir, it reacts with the carbonate constituents of rock and is consumed, raising the *p*H of brine. As the *p*H increases, the polymer microgels swell and increase viscosity of polymer-containing water. As developed in detail in Huh *et al*. (2005), the Carreau model is employed to describe the dependence of polymer viscosity on *p*H, polymer concentration, and Darcy velocity:

$$\mu - \mu_\infty = (\mu_o - \mu_\infty)\left[1 + (\lambda_{eff}\gamma)^\alpha\right]^{(n-1)/\alpha} \qquad \text{[VII.16]}$$

where μ_o and μ_∞ are the limiting Newtonian viscosities at the low and high shear limits, respectively; λ and n are polymer-specific empirical constants; α is generally taken to be 1.5; and γ_{eff} is effective shear rate which is given in terms of Darcy velocity and permeability (Huh *et al*. 2005). In Eq.[VI.16], μ_o is given in terms of the polymer and H^+ concentrations, and μ_∞ is usually assumed to be $\mu_\infty \approx \mu_{wo}$.

VI.4. Solution Method for the Transport Equations

In order to solve the above equations, we will first put them in dimensionless forms. For the computational convenience, the following independent variables are employed:

$$x \equiv \ell n\left(\frac{r}{r_w}\right); \qquad \tau \equiv \frac{t u_w}{r_w}$$

where $u_w \equiv \frac{Q_t}{2\pi r_w H}$

Eq.[VI.10] then becomes

$$\phi \frac{\partial C_{hi}}{\partial \tau} + U_i e^{-x} \frac{\partial C_{hi}}{\partial x} = \lambda_h e^{-2x} \frac{\partial^2 C_{hi}}{\partial x^2} + \sum_{j=1}^{N} N_{Dj} C_{hi}(C_{je} - C_{ji}) \qquad \text{[VII.17]}$$

where

$$U_i \equiv \frac{u_i}{u_w} = \frac{f_{ni}\,\ell n\left(\frac{r_o}{r_w}\right)}{\left(\frac{h_i r}{H r_w}\right)\int_{r_w}^{r_o}\left(\frac{\mu_i}{\mu_{wo}}\right)\frac{dr}{r}} = \frac{f_{ni} x_o}{\left(\frac{h_i}{H}\right) e^x \int_0^{x_o}\left(\frac{\mu_i}{\mu_{wo}}\right) dx} \qquad \text{[VII.18]}$$

with $x_o \equiv \ell n\left(\frac{r_o}{r_w}\right)$; and $\lambda_h \equiv \frac{D_h}{r_w u_w}$ is the dispersivity; and

$$N_{Dj} \equiv \frac{r_w R_j S}{u_w} = \frac{(r_w / u_w)}{(1/R_j S)} \qquad \text{[VII.19]}$$

is the Damkohler number, which is the ratio of the convection residence time to the reaction time.

Eqs. [VII.11], [VII.13] and [VII.14] become, respectively,

$$\phi \frac{\partial C_{ji}}{\partial \tau} = -N_{Dj} C_{hi} (C_{je} - C_{ji}) \qquad \text{[VII.20]}$$

$$\phi \frac{\partial C_{ti}}{\partial \tau} + U_i e^{-x} \frac{\partial C_{ti}}{\partial x} = \lambda_t e^{-2x} \frac{\partial^2 C_{ti}}{\partial x^2} \qquad \text{[VII.21]}$$

$$(\phi + \frac{\partial A_i}{\partial C_{pi}}) \frac{\partial C_{pi}}{\partial \tau} + U_i e^{-x} \frac{\partial C_{pi}}{\partial x} = \lambda_p e^{-2x} \frac{\partial^2 C_{pi}}{\partial x^2} \qquad \text{[VII.22]}$$

where

$$\frac{\partial A_i}{\partial C_{pi}} = \frac{a_1}{(1 + a_2 C_{pi})^2} \qquad \text{[VII.23]}$$

The above equations are in the form

$$\frac{\partial C}{\partial \tau} = b_1 \frac{\partial^2 C}{\partial x^2} + b_2 \frac{\partial C}{\partial x} + b_3 C \qquad \text{[VII.24]}$$

This can be expressed in finite-difference form

$$\frac{C_k - C'_k}{\Delta \tau} = \frac{b_1}{\Delta x^2}\left(C_{k+1} - 2C_k + C_{k-1}\right) + \frac{b_2}{\Delta x}\left(C_k - C_{k-1}\right) + b_3 C_k \qquad \text{[VII.25]}$$

Where, $\Delta\tau$ and Δx are time-step size and gridblock size, respectively; C_k is the current time-step value of C at the k-th gridblock; and C'_k is the known, previous time-step value of C. Eq.[VII.25] can be re-arranged as

$$\left(\frac{b_1}{\Delta x^2} - \frac{b_2}{\Delta x}\right) C_{k-1} + \left(-\frac{2b_1}{\Delta x^2} + \frac{b_2}{\Delta x} + b_3 - \frac{1}{\Delta \tau}\right) C_k + \left(\frac{b_1}{\Delta x^2}\right) C_{k+1} = -\frac{C'_k}{\Delta \tau} \qquad \text{[VII.26]}$$

This, when collected for all gridblocks, forms a tri-diagonal matrix, and can be solved by simple matrix inversion.

In solving the above array of finite-difference equations for H^+ (Eq.[VII.18]), polymer (Eq.[VII.23]), mineral ions (Eq.[VII.20]), and tracer (Eq.[VII.21]), the following initial and boundary conditions are needed.

(a) Initial conditions in the reservoir (for all k for $t = 0$)

$$C_{hi} = C_{hr};\ \ C_{pi} = 0;\ \ C_{ti} = 0_r;\ \ C_{ji} = C_{je}$$

where C_{hr} is the resident brine's H^+ concentration; and C_{je} is the equilibrium concentration of the j-mineral anion.

(b) Boundary conditions at the injection well (for $k = 0$)

$$\begin{array}{ll} C_{hi} = C_{ho} & \text{for } t > 0 \\ C_{pi} = 0 & \text{for } t_1 > t > 0 \\ C_{pi} = C_{po} & \text{for } t \geq t_1 \\ C_{ti} = C_{to} & \text{for } t > 0 \\ C_{ji} = 0 & \text{for } t > 0 \end{array}$$

where C_{ho} is the injection brine's H^+ concentration; t_1 is the pre-flush period; and C_{po} is the injection polymer concentration. The injection brine does not contain any mineral anions.

(c) At the reservoir's outer boundary (k = K+1), the approximation that the material flux remains constant is imposed:

$$\frac{C_{K+1} - C_K}{\Delta x} = \frac{C_K - C_{K-1}}{\Delta x}$$

Based on the derivation, a preliminary version of the Fortran program is being developed.

VI.5. Near-Term Tasks

Earlier, Reznik *et al*. (1984) and Sorbie and Mackay (2005) investigated how the injection of a high-viscosity fluid into a multi-layer heterogeneous reservoir, that contains a low-viscosity fluid, alters the injection allocation. They found that, if there is no crossflow among the layers, the reduction in injection allocation disparity is not long-lasting, contrary to the common perception. Our first task is to investigate whether such is also true with injection of the *p*H-sensitive polymer.

Our second task is to explore the possibility of developing computer software that helps optimize the vertical conformance control application of the *p*H-sensitive polymer. In applying the *p*H-sensitive polymer technique, we envision a two-step process. The first step is to simply inject a weak acid for a brief period of time, produce back, and analyze the effluent ion contents. The intent of this test is to characterize the mineral composition of the reservoir that affects the *p*H evolution when acid is later injected with polymer. The second step is the injection of a pre-flush bank of acid, followed by a bank of polymer solution in an acidic condition. It is hoped that the optimization program can help design an effective way of injecting the acid and polymer banks.

References

Huh, C., Choi, S. K., and Sharma, M. M., "A Rheological Model for pH Sensitive Ionic Polymer Solutions for Optimal Mobility Control Applications", **SPE 96914** presented at **SPE Annual Tech. Conf.**, Dallas, TX, Oct. 9-12, 2005.

Reznik, A. A., Enick, R. M., and Panvelker, S. B., "An Analytical Extension of the Dykstra-Parsons Vertical Stratification Discrete Solution to a Continuous, Real-Time Basis", **Soc. Petrol. Eng. J.,** 643-656, Dec. 1984.

Sorbie, K. S., and Mackay, E. J., "Scale Inhibitor Placement: Back to Basics—Theory and Examples", **SPE 95090** presented at **SPE Intern. Symp. Oilfield Scale**, Aberdeen, United Kingdom, May 11-12, 2005.